Sādhanā, Vol. 23, Parts 5 & 6, Oct & Dec 1998, pp. 505–539. © Indian Academy of Sciences

LDA measurements and CFD simulations of flow generated by impellers in mechanically agitated reactors

J B JOSHI*, A K SAHU and P KUMAR

Department of Chemical Technology, Chemical Engineering Division, University of Mumbai, Matunga, Mumbai 400 019, India
e-mail: jbj@udct.ernet.in

Abstract. The turbulent flow produced by various designs of axial flow impellers in a stirred vessel was measured using a laser Doppler anemometer (LDA). Flat-bottomed cylindrical vessels of diameters 0.3 m and 0.5 m provided with 4 baffles of $T/10$ width were used as the reactors. The standard two-equation (k-ϵ) turbulence model was used to numerically simulate the flow (both 2D and 3D). Three numerical schemes, namely upwind scheme, hybrid scheme and power-law scheme, were used to evaluate the competitiveness of the various schemes. The effects of the initial guess values of the flow variables, the under-relaxation parameters and internal iterations etc. on the rate of convergence were analysed for both 2D and 3D models. The effect of grid size was also studied in both the cases. The 2D and 3D predictions were compared and it was observed that the 2D predictions were not good enough to give the details of the flow. So, the sensitivity of the model parameters on the flow characteristics was investigated thoroughly in the case of 3D models. It was observed that no single set of model parameters could yield even reasonable agreement between the model predictions and the experimental observations throughout the vessel. Therefore, the concept of zonal modelling was introduced for the r-z plane. It was observed that with the introduction of zonal modelling the predicted values of flow variables were in good agreement with experimental data even close to the top surface of the tank. The same could not be obtained with a standard set of parameters and single zone.

Keywords. LDA measurements; CFD; turbulence parameters; zonal modelling; mechanically agitated reactors; pitched blade turbine.

*For correspondence
A list of symbols and abbreviations used in the paper is given at the end

1. Introduction

Stirred tank reactors are used for many operations in the chemical, petrochemical and biochemical industries. Different types of impellers are used in the stirred reactors depending on the process objective. The knowledge of the flow pattern produced by the impeller is essential because the selection of the impeller for a specific process objective is decided by the flow pattern. Experimental investigations of flow patterns in mechanically agitated tanks with pitched-blade turbine downflow (PTD) have been extensively carried out during the last thirty years. The salient features of the measurements for PTD by several authors have been given in table 1. In the beginning, measurement was confined to mean velocity profiles only. With the advent of modern measurement techniques such as laser Doppler anemometry, it is possible to measure the turbulent flow characteristics along with the mean velocity profiles. In the past, the prime interest of experiment was to find the flow pattern in the vicinity of the impeller. However, for reliable design, knowledge of the flow pattern and turbulent flow characteristics in the entire flow domain is indispensable. In most of the published work (Ranade & Joshi 1989; Kresta & Wood 1993; Fokema *et al* 1994; Ranade & Dommeti 1996; Xu & Mcgrath 1996) experimental data and/or model predictions were reported in the region close to the impeller. Further, measurements regarding turbulent flow characteristics such as turbulent stresses and turbulent energy dissipation rate were also not made for the pitched-blade impeller.

1.1 *Review of experimental work*

Tatterson *et al* (1980) observed the general nature of flow using the stereoscopic visualization technique for a bench scale and an industrial scale pitched-blade turbine. They observed that flows were not similar. In the flow produced by the bench-scale pitched-blade turbine, the high speed jet was dominant and the trailing vortex was weak. On the other hand, the industrial-scale pitched-blade turbine produced a predominant trailing vortex system. Fort (1986) measured the axial velocity profile just above and below the impeller, using a pitot tube, for a pitched-blade turbine. It was found that below the impeller, between the downward and upward flowing streams, the axial velocity was very low and the size of this region depended on the number of blades and the blade angle. He also measured the primary flow number and expressed it in terms of D/T ratio and off-bottom clearance for different axial flow impellers. Hydraulic efficiency was found to increase with a decrease in the D/T ratio for a pitched-blade turbine with blade angle 45° and off-bottom clearance $H_c/T = 1/4$. Ranade & Joshi (1989) made detailed investigation of flow generated by pitched-blade turbine and the influence of various geometrical parameters on the flow. They found that the mean velocities and the turbulent intensities were proportional to the impeller speed within the range studied (impeller Reynolds number: 4×10^4–1.4×10^5). They observed that while small impellers generated strong downward flow, large impellers ($D/T = 0.5$) generated radially outward flow through the vertical periphery of the impeller swept surface. Hydraulic efficiency increased with an increase in the blade angle and also with an increase in the D/T ratio. Blade width of 0.3D was found to be optimum from the point of view of hydraulic efficiency and primary pumping capacity.

Table 1. Experimental details.

Author(s)	Measurement technique	Vessel dimension T (mm)	Impeller type, dimension and location	Range of measurement		Remarks
				Radial	Axial	
Fort (1967)	Photographic method	290	Propeller, $D = 72.5$ mm, 96.6 mm, $H_c/T = 0.155$ 0.25, 0.333, 0.431,	–	–	Measurement made close to the impeller only
Fort *et al* (1971)	Pitot tube	290	Paddle, $D = 96.66$ mm, 72.5 mm, 58 mm, $H_c/T = 1/4$	Up to the wall	Just below and above the impeller	
Tatterson *et al* (1980)	Stereoscopic visualization	295, 914	PTD, $D = 102$ mm, 305 mm, $H_c/T = 1/3$	–	–	Only general nature of flow observed
Ranade & Joshi (1989)	LDA	300, 500	PTD, $D = 75$ mm, 100 mm, 150 mm, 167 mm, $H_c/T = 1/3$, 1/4, 1/6	Up to $r = 0.95$	Up to 20 mm above the bottom and above the impeller up to $z = 0.74$	
Fort *et al* (1991)	LDA	297	PTD, $D = 99$ mm, $H_c/T = 1/3$	Up to the wall	Just below and above the impeller blade	
Jaworski *et al* (1991)	LDA	146	PTD, $D = 48.67$ mm, $H_c/T = 1/2$, 1/4	Up to $r = 0.96$	Up to 6 mm above the bottom and up to 56.5 mm above the impeller	
Ranade *et al* (1991)	LDA	300, 500	PTD, $D = 75$ mm, 100 mm, 150 mm, 167 mm, $H_c/T = 1/3$, 1/4, 1/6	Up to $r = 0.95$	Up to 20 mm above the bottom and $z = 0.66$ above the impeller	Data from Ranade & Joshi (1989)
Ranade *et al* (1992)	LDA	500	PTD with blade angles 30, 45, 60°, and five other designs of axial flow impellers, $D = 167$ mm, $H_c/T = 1/2$	Up to $r = 0.95$	Up to $z = 0.37$ below the impeller and up to $z = 0.2$ above the impeller	
Kresta & Wood (1993a)	LDA	152.4	PTD, $D = 76.2$ mm, 50.8 mm, H_c/T varied from 1/2–1/20	Up to $r = 1$	Up to 40.4 mm below the impeller	

(*Continued on next page*)

Table 1. (*Continued*)

Author(s)	Measurement technique	Vessel dimension T (mm)	Impeller type, dimension and location	Range of measurement		Remarks
				Radial	Axial	
Kresta & Wood (1993b)	LDA	152.4	PTD, $D = 76.2$ mm, $H_c/T = 1/4$	Up to $r = 0.58$	At 2 mm below the lower edge of the impeller blade	
Bakker & Van den Akker (1994)	LDA	444	PTD, A315, $D = 177.6$ mm, $H_c/T = 0.3$.	–	–	
Fokema *et al* (1994)	LDA	150	PTD, $D = 75$ mm, $H_c/T = 0.465$, 0.25	Up to $r = 1$	Up to 32.3 mm below the impeller	
Sahu & Joshi (1995)	LDA	500	PTD1, PTD2, CURPTD, MODPTD, PROP, MPTD, $D = 167$ mm, 155 mm (PTD2), $H_c/T = 1/2$	Up to $r = 0.95$	Up to $z = 0.52$ below the impeller and up to $z = 0.56$ above the impeller	Data from Ranade *et al* (1992)
Armenante & Chou (1996)	LDA	290	PTD, $D = 102$ mm, $H_c/T = 0.414$	Up to $r = 0.85$	Above up to 169 mm, and below up to 82.8 mm	
Harris *et al* (1996)	LDA	300	PTD, $D = 75$ mm, 100 mm, 150 mm, 167 mm, $H_c/T = 1/3$, 1/4, 1/6	Up to $r = 0.95$	Up to 20 mm above the bottom and up to $z = 0.366$ above the impeller	Data from Ranade & Joshi (1989)
Hockey & Nouri (1996)	LDA	294	PTD, $D = 98$ mm, $H_c/T = 1/3$	Up to $r = 0.83$	–	
Ranade & Dommeti (1996)	LDA	300	PTD, $D = 100$ mm, $H_c/T = 1/3$	Up to $r = 0.95$	Up to 20 mm above the bottom and up to $z = 0.366$ above the impeller	Data from Ranade & Joshi (1989)
Xu & Mcgrath (1996)	LDA	305	PTD, $D = 101.67$ mm, $H_c/T = 1/3$	Up to $r = 0.5$	Above the impeller up to 3 mm and below up to 49 mm	

Fort *et al* (1991) measured the radial profiles of the axial and radial components of the mean velocity below and above a four-blade pitched blade turbine. Below the impeller, they measured the velocities up to very close to the vessel bottom. They calculated the turbulence characteristics, Reynolds stress ($\overline{u'v'}$) and eddy viscosity using these radial profiles according to von Karman's hypothesis applied to axially symmetrical systems with cylindrical coordinates. They found that while the radial component of the mean velocity exhibited rather flat profiles, the axial component exhibited significant slopes. Reynolds stress and eddy viscosity below the impeller were found to be much bigger than those above the impeller.

Jaworski & Fort (1991) measured the flows produced by three different sizes of pitched blade turbines using pitot tubes at four axial levels. They used the data to derive the radial and axial component of mean velocity, static and total pressures. They confirmed the independence of the dimensionless mean velocities on the impeller speed. It was found that all the variables diminished when the impeller diameter was decreased. They also derived expressions to calculate the integral values of the volumetric and energy flow rate at different axial levels. The energy dissipation above the impeller was smaller than that below the impeller.

Jaworski *et al* (1991) investigated the turbulent flow produced by a 45° pitched blade turbine impeller of diameter equal to one-third of the vessel diameter for two off-bottom clearances of $H/4$ and $H/2$. They found that the off-bottom clearance influenced the flow near the vessel bottom. At the mid-height impeller location, a low intensity flow reversal was observed over the entire vessel base, whereas in case of the one-third off-bottom clearance, flow reversal was present only near the axis. They found the flow to be generally isotropic and homogeneous except in the impeller outflow stream. They also compared the turbulent fluctuations by the pitched blade turbine to that generated by a disc turbine and found it to be close. This work was found to be broadly in agreement with a similar work by Ranade & Joshi (1989).

Kresta & Wood (1993a) compared the various methods available for the estimation of turbulent energy dissipation rate (ϵ). The system used was a four-blade 45° pitched blade turbine rotating in a cylindrical fully baffled tank with velocity measurements by laser Doppler anemometry. They made measurements at the lower edge of the impeller blade. Various corrections were suggested for all these methods and the dimensional argument and autocorrelation methods were found to be reliable and practical. Kresta & Wood (1993b) studied the effect of off-bottom clearance on the circulation pattern for two sizes of pitched blade turbine. They observed a counter rotating secondary circulation loop close to the bottom of the tank for an off-bottom clearance of $T/2$. The main circulation loop did not extend to the top of the tank when the clearance was $T/3$. For all cases their results showed that the main circulation loop was much smaller than that portrayed by the conventional view. When the off-bottom clearance was increased the impeller discharge flow was deflected towards the horizontal for the impeller having diameter equal to $T/2$. But the $T/3$ impeller, since the secondary circulation loop was not as strong, did not affect the angle of the impeller discharge.

Hockey & Nouri (1996) quantified the power characteristics of a 60° six-blade pitched blade turbine as a function of Reynolds number. The power number decreased rapidly by 12% at a Reynolds number of 1200 and was constant at 2.25 at high Reynolds numbers.

It was observed that flow in the impeller discharge stream was anisotropic and isotropic in the rest of the vessel. A stronger recirculation region close to the vessel bottom in the central region was evident. The mass balance in and out of the impeller was within 1%. The kinetic energy balance around the impeller showed that less than 6% of the input energy was dissipated within the impeller region. They also compared this pitched blade turbine with a Rushton turbine of the same diameter and found that the pitched blade turbine generated 2.5 times more mean flow per unit power input, converted the same amount of energy into turbulence and dissipated less energy in the impeller.

1.2 *Review of CFD modelling*

To obtain flow characteristics in the entire vessel by experiment is not an easy task. Therefore, attempts are being made to generate turbulent flow profiles in a stirred vessel by developing mathematical models. The accuracy of mathematical modelling of the flow in an agitated tank depends on the degree of sophistication of the model. For the sake of simplicity various analytical models (Desouza & Pike 1972; Drbohlav *et al* 1978 ; Platzer & Noll 1981; Fort 1986) were devised to predict the mean flow velocities. However, these simplified models did not display the turbulent characteristics of flow patterns. Development of some effective turbulent models such as k-ϵ and algebraic stress models, led researchers (Placek *et al* 1978; Platzer 1981; Harvey & Greaves 1982) to present the numerical solution of the fully turbulent flow in a baffled stirred tank. For the sake of brevity, a brief account of the simulation of stirred vessels with PTD has been given in table 2. However, it is of interest to highlight the contribution of various research workers and the shortcomings of the various turbulent models.

Pericleous & Patel (1987) simulated a stirred biochemical reactor which contained two tangential and one axial impellers, heating coil arrangements around its periphery and a sparger ring for introducing air. They solved the Navier–Stokes equations using the commercial code PHOENICS. Impellers were considered the sources of the momentum and the other geometrical features, its sinks. They also simulated gas bubble distribution in the vessel. Velocity profiles at selected locations were compared with the experimental data which exhibited reasonable agreement.

Ranade and coworkers (Ranade & Joshi 1989; Ranade *et al* 1989) analysed the influence of grid size, impeller boundary conditions and values of model parameters on the predicted flow. The boundary conditions were specified on the bottom impeller swept surface and linear profiles were used for all the variables except radial velocity. They observed that the location of maxima in axial velocities in predicted flow did not move away from the axis of symmetry as axial location approaches the vessel bottom unlike the experimental data. Below the impeller, the model overpredicted the axial velocity. They believed that the absence of vortices behind the baffles was not the shortcoming of the model but of the computational resources. Turbulent kinetic energy was overpredicted near the vessel bottom and energy dissipation rate was not verified since the experimental data were not available. However, they accounted for 90% of the input energy. Based on the suggestions made by Abujelala & Lilley (1984), they reported that, with the variation of parameter values C_2 and C_D, the overall error between the experimental data and the predictions could be minimised. But detailed optimisation of the model parameters was not attempted.

Table 2. Numerical details.

Author	Model	Algorithm	CFD code	Scheme	Grid size (r, θ, z)	Range of prediction		CMV made	CTP made	P_p/P_e
						Radial	Axial			
Pericleous & Patel (1987)	–	SIMPLEST	PHOENICS	–	–	Up to $r = 0.2$	Up to 50 mm above the impeller and 50 mm below the impeller	u, v	–	–
Ranade *et al* (1989)	k-ϵ	SIMPLER	In-house	Power-law	$30 \times 5 \times 46$	Up to $r = 0.96$	Up to $z = 0.366$ above the impeller and up to $z = 0.533$ below the impeller	u, v, w	k	0.9
Ranade *et al* (1991)	k-ϵ	SIMPLER	In-house	Power-law	$15 \times 16 \times 31$	Up to $r = 0.96$	Up to $z = 0.366$ above the impeller and up to $z = 0.533$ below the impeller	u, v, w	k	0.9
Ranade *et al* (1992)	k-ϵ	SIMPLER	In-house	Power-law	$30 \times 5 \times 46$	Up to $r = 0.95$	Up to $z = 0.2$ above the impeller and up to $z = 0.37$ below the impeller	u, v, w	k	–
Bakker & Van den Akker (1994)	k-ϵ and ASM	–	FLUENT	Power-law	$25 \times 25 \times 40$	–	–	v	u'	–
Fokema *et al* (1994)	k-ϵ	SIMPLEC	FLOW3D	Hybrid	$20 \times 20 \times 43$ (non-uniform)	Up to $r = 1$	Up to 32.34 mm below the impeller	v	k, ϵ	–
Sahu & Joshi (1995)	k-ϵ	SIMPLE	In-house	Power-law, hybrid, upwind	28×33 (r, z)	Up to $r = 0.96$	Up to z = 0.56 above the impeller and up to $z = 0.52$ below the impeller	u, v	k	1.6
Armenante & Chou (1996)	k-ϵ and ASM	–	FLUENT	–	(24, 696) node points	Up to $r = 0.95$	Up to 169.2 mm above the impeller and up to 82.8 mm below the impeller	u, v, w	k, ϵ	0.11
Harris *et al* (1996)	k-ϵ and Reynolds stress	–	FLOW3D	–	$60 \times 16 \times 58$	Up to $r = 0.95$	Up to $z = 0.366$ above the impeller and up to $z = 0.533$ below the impeller	u	k	–
Ranade & Dommeti (1996)	k-ϵ	–	FLUENT	–	$35 \times 38 \times 46$	Up to $r = 0.95$	Up to $z = 0.366$ above the impeller and up to $z = 0.533$ below the impeller	u, v, w	–	0.8
Xu & Mcgrath (1996)	Reynolds stress	–	FLOW3D	–	–	Up to $r = 0.5$	Up to 3 mm above the impeller and up to 49 mm below the impeller	u, v, w	–	1.1

Ranade *et al* (1991) simulated the flow produced by a pitched blade turbine using standard k-ϵ model and extended the results to study the mixing characteristics of pitched blade turbines. The k-ϵ model promisingly reproduced the major characteristics of the flow, despite strong anisotropy. The model overpredicted k near the vessel bottom. Simulated mixing performance also agreed well with the experimental data. Ranade *et al* (1992) studied the effects of the shapes of eight axial flow impellers (including PTD) on the flow generated in agitated vessels. They found that the two equation (k-ϵ) model was adequate for predicting the bulk flow in the case of all the impellers. They compared the impellers in terms of mean velocities, turbulent kinetic energy, pumping effectiveness and hydraulic efficiency.

Bakker & Van den Akker (1994) provided turbulence profiles at the bottom surface of the impeller according to their experimental data. As the measurement of the radial component was not possible, the experimental k value was assumed to be equal to three-fourths of the squares of axial and tangential components of the RMS velocity. Measurements were made at three tangential locations with both zero baffle-wall spacing and with baffle-wall spacing equal to 0.023T. Flow pattern was found to be very different in these two cases. However, a secondary circulation was observed in both cases in the upper part of the vessel. Only axial velocity was compared at various axial locations and agreement was good in the region below the impeller. However, above the impeller, the discrepancy was of high magnitude. Bakker & Van den Akker (1994) illustrated the anisotropy of turbulent flow by comparing the values of RMS velocity predicted by ASM and the k-ϵ model. They observed that the result obtained by ASM agreed well with experimental data as compared to the values predicted by the k-ϵ model. It was also observed that the values of energy efficiency predicted by the k-ϵ model were significantly lower than that with the ASM.

Fokema *et al* (1994) analysed the importance of specifying proper boundary conditions for the prediction of flow characteristics by using two sets of data obtained from two different off-bottom clearances. They modelled the impeller using a thin disk with inlets across both surfaces. The velocity and turbulent quantities measured at the impeller discharge were specified at both lower and upper surfaces of the impeller. The disk was made as thin as possible in order to minimise the error introduced by using only the discharge boundary conditions on both the surfaces. The boundary conditions for turbulent kinetic energy and its dissipation rate were obtained by using the method recommended by Kresta & Wood (1993b). A body-fitted coordinate system was employed for simulating the flow. The grid system was non-uniform in the axial and tangential directions in order to take into account the steep variation near the impeller and baffle. They verified the presence of a secondary circulation loop when the ratio of impeller bottom clearance to impeller diameter was greater than 0.6. For axial velocity, the agreement between the predicted and the experimental values was found to be excellent. However, the comparison was presented for a region close to the impeller and no comparison was made near the wall. The predicted energy dissipation rate profiles immediately below the impeller were of the correct magnitude and attained peak values just beyond the tip of the impeller. However, as one moved away from the impeller, the predicted values of ϵ were found to decay to only a fraction of the experimental values. This underprediction of dissipation rate was also observed above the impeller. By using high clearance boundary condition for low clearance, it was found that the experimentally determined boundary condition must only

be used in simulations where the tank geometry is similar to the experimental case. It was observed that correct specification of the axial and tangential velocity components was required to generate correct velocity field for a given geometry. It was also observed that the ratios of average dissipation rate in the impeller region to that in the tank were 5.3 and 5.9 for the high and the low clearance cases respectively. These findings were in good agreement with those experimentally determined by Jaworski & Fort (1991).

Sahu & Joshi (1995) reviewed the literature and pointed out the need to study the effect of various numerical schemes, initial guess values of the flow variables, underrelaxation parameters, internal iterations etc. on the rate of convergence and the effect of model parameters on the flow variables. Further, they investigated the effect of the global grid size and near-wall grid size on the solution. They studied six designs of axial flow impeller. Although the upwind scheme took less computing time, it underpredicted the flow variables. Solution obtained by power-law and hybrid schemes were almost the same and there was no significant difference in the computational time between these two schemes. Therefore, for the robustness of the algorithm, they decided to use the power-law scheme. For solving algebraic equations iteratively it was observed that a line by line TDMA method was more efficient than the Gauss–Siedel method. Introduction of a fine grid system near the wall had an effect in the near-wall region as well as in the bulk region. The behaviour of the predicted values of k for a fine grid size near the wall was in conformity with the experimental data. Below the impeller, one subdivision of near-wall control volume gave a grid-independent solution, whereas in the upper part of the vessel three to four subdivisions were necessary to obtain a grid-independent solution. This variation was attributed to the small magnitude of turbulent kinetic energy in this region. Sahu & Joshi (1995) compared predicted flow variables (axial velocity, radial velocity, k) with the experimental results for two different values of C_D (0.05, 0.09). They observed that there was a qualitative agreement between the predicted and experimental results in the impeller region whereas away from the impeller, particularly in the upper part of the vessel, differences were large.

In a recent study, Armenante & Chou (1996) opined that the use of the isotropic turbulence model and the specification of experimental data only on the bottom surface of the impeller-swept volume are probably the limitations of previous CFD analyses. They concluded that better results could be obtained by providing boundary conditions both below and above the impeller-swept region. The velocity profiles in the impeller region were found to be flatter than those reported earlier (Ranade *et al* 1989; Kresta & Wood 1993b). They attributed this discrepancy to the difference in the impeller clearance, the D/T ratio and the baffling system (in the earlier studies baffles extended up to the vessel bottom, but in this work a gap existed between baffles and the vessel bottom). Turbulent kinetic energy profiles in the impeller region were also flatter than those reported by other investigators (Ranade & Joshi 1989; Ranade *et al* 1992; Kresta & Wood 1993a) who showed the existence of a peak at $r/R = 0.5$. They observed that, outside the impeller region for all the three components of velocity, simulations based on two location boundary conditions and ASM were superior. In the upper part of the vessel, a wide difference between the experimental and predicted values was found, irrespective of the model. However the difference between the predicted values of ASM and k-ϵ was very small.

Harris *et al* (1996) reviewed the recent progress in the predictions of flow in baffled stirred tank reactors. They found that the comparison between 3D simulation predictions

and the experimental results reported in the literature exhibited generally good agreement for the radial and axial components of mean velocity, while the tangential component was less well-predicted, with anisotropic models yielding superior results. One area of major concern has been the prediction of turbulent quantities especially ϵ. Some of the work in the literature yielded good results in the impeller stream, elsewhere in the vessel predictions were generally poor. They carried out simulations both by the inner-outer method and by providing impeller boundary conditions. In the inner-outer approach, a fictitious cylindrical boundary was selected with a radius intermediate between that of the impeller tip and the baffle inner edge. The flow solution over the surface was azimuthally averaged. The resulting values were used as the outer boundary condition for a second simulation in a rotating frame. This iterative procedure was applied till a converged steady state solution was obtained (Brucato *et al* 1994). In the simulation using boundary conditions, mean radial velocities were in good agreement with experimental results. The most important observation was that both models yielded similar predictions. In both models, the turbulent kinetic energy and its dissipation rate were underpredicted in the impeller stream. It was interesting to note that the inner zone simulation yielded values of k in much closer agreement with the experimental data below the impeller than the simulation using impeller boundary conditions. The predicted mean tangential velocity was in good agreement with experimental observations. Just below the liquid surface, the k-ϵ model predicted that most of the fluid was swirling in the opposite direction to the impeller.

Ranade & Dommeti (1996) emphasized the importance of flow predictions without supplying boundary conditions by giving the following reasons: (i) In the black box treatment, data for a particular configuration cannot be used to screen a large number of alternative mixer configurations, (ii) getting the boundary conditions in the case of multiphase flow is not feasible, (iii) the black box approach cannot capture the flow details between the impeller blades. Ranade & Dommeti (1996) employed a snapshot approach. Once the flow in a baffled stirred vessel became fully developed, the flow pattern in the impeller region was periodic. For such a case, a snapshot of this flow (solution at any particular instant) can describe the flow within the impeller blades with sufficient details. By inspecting the magnitude of various terms in the governing transport equations, the authors observed that the time derivative terms were small compared to the convective and other terms, and hence could be ignored. However, near the impeller swept volume, this assumption might not hold good. Therefore, the periodic nature of the flow was used to reformulate the time derivatives in terms of spatial gradients. In the case of axial velocity, comparison between the prediction and the experimental data was quite adequate, except for the disagreement near the symmetry axis. For radial and tangential velocities, predictions at locations away from the impeller were also closer to the experimental data. Close to the impeller, both the radial and the tangential velocities were overpredicted. Away from the impeller, the predicted tangential velocity showed a counter rotating region near the symmetry axis which was not observed in experiments. A comparison of the predicted values of gross parameters such as pumping number and power number was also made with the published data. The predicted value of primary pumping number was 0.85, whereas Ranade & Joshi (1989) reported this value as 0.93. They reiterated that the agreement could be said to be adequate considering the *a priori* nature of the predictions and predicted flow between the impeller blades for the first time.

Xu & Mcgrath (1996) used the momentum source and sink technique to evaluate the impeller boundary conditions. According to this technique the impeller blades usually having a continuous contour were replaced with finite blade sections by dividing the blade into a number of vertical strips from the hub to the tip. The blade section inside each strip was approximated to an aerofoil and aerofoil aerodynamics was applied. The predicted values were very good for the axial and radial velocities, whereas the tangential velocity was overpredicted. However, the results were presented in the region very close to the impeller. Therefore, the reliability of the method for regions away from the impeller could not be ascertained. Xu & Mcgrath (1996) concluded that the predicted values obtained by the momentum source–sink method were as good as those predicted by using the LDA data as boundary conditions.

From the above discussion it is clear that the comparison between the experimental findings and the numerical predictions was generally inadequate except in regions close to the impeller irrespective of the mathematical model and the method used for simulation of the impeller boundary conditions. It is well-known that, for numerical simulation of flow in a stirred tank, the turbulence parameter values are kept the same as that of pipe flow. Since in a stirred vessel the flow pattern is entirely different from that in a pipe, the turbulence parameter values may need modification in conjunction with experimental data to yield better predictions. Therefore, optimisation of parameters related to stirred tanks is required. However, it was observed that a single set of model parameters did not give good predictions in the entire vessel for all the flow variables. It was concluded that the discrepancy may be the shortcoming of the turbulence models.

Although a universal turbulence model is a distant dream, it was shown by Ferziger *et al* (1988) that a turbulence model could be made universal with the introduction of zonal modelling. The philosophy of zonal modelling is as follows. With the knowledge of flow pattern, the flow domain is divided into various sub-domains. Each sub-domain may be called a zone. In each zone, an optimal set of model parameters is chosen and at the interface care is taken to maintain the continuity. In this way, the agreement between experimental observations and model predictions could be improved for all the flow variables in the entire flow domain. Therefore, in the present work, the k-ϵ model with zonal modelling has been used to simulate the flow produced by a pitched downflow turbine impeller.

2. Laser Doppler anemometer set-up, stirred vessel and impellers

The Laser Doppler anemometer (LDA) set-up comprised a Dantec 55X modular series LDA and its associated electronic instrumentation and a personal computer. The LDA was operated in a forward scatter mode. Figure 1a shows the experimental arrangement. A 5W Ar-ion laser (made by Spectra Physics, USA) was used as the laser source. The laser and optics were mounted on a bench which had a unidirectional traversing mechanism. This mechanism could displace the front lens by ± 200 mm in 5μm increments by means of a linearly encoded stepper motor (which can be monitored either by computer or manually). To identify the flow reversals correctly, a frequency shift was given to one of the beams by means of a Bragg cell with electronic down mixing. Data validation and signal processing were carried out with the help of a Dantec 57N10 Burst Spectrum Analyser (BSA). A

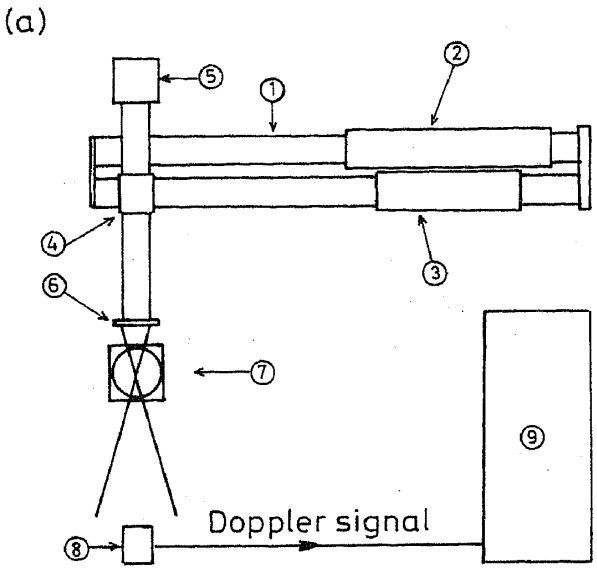

No.	Description
1	Mounting bench
2	5W Ar-ion beam
3	Optics
4	Mirror
5	Traversing unit
6	Front lens
7	Tank
8	Photomultiplier tube
9	LDA signal processor (BSA) with PC/AT 386 computer

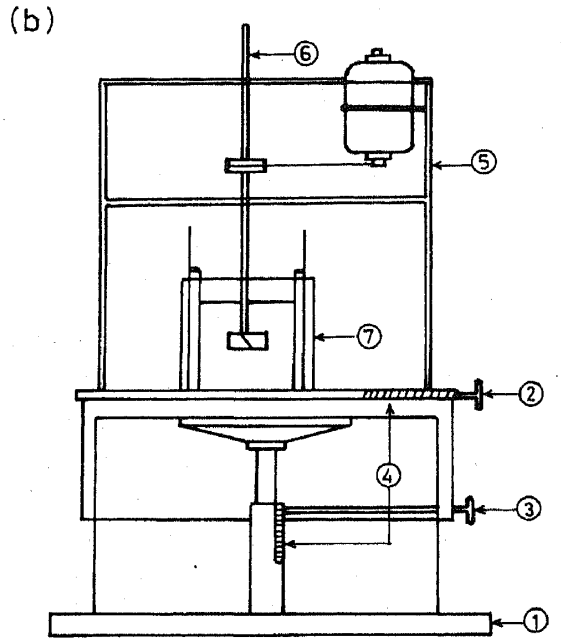

No.	Description
1	Screw-jack
2	Wheel for horizontal movement
3	Wheel for vertical movement
4	Scale
5	Agitator mount assembly with motor
6	Agitator shaft assembly with pulleys
7	Tanks

Figure 1. (**a**) Experimental arrangement of LDA. (**b**) Schematic diagram of the agitation set-up.

personal computer functioned as the central data acquisition and reduction controller via an interface (National Instruments PC2A Card). Further details have been given by Ranade *et al* (1992) and Ranade & Joshi (1990).

The basic components of the agitation set-up are shown in figure 1b. It consists of a 1 HP variable speed DC motor and shaft. The entire agitation assembly was mounted on a table with a two-dimensional (r, z) traversing mechanism. The traversing system could displace the entire assembly in a ± 250 mm range in 1 mm increments along the r and z co-ordinates. Flat-bottomed cylindrical vessels of diameter 0.3 m and 0.5 m provided with 4 baffles of $T/10$ width were used as the reactors. To eliminate the effect of vessel curvature on the intersecting laser beams, the vessels were placed in square vessels of side

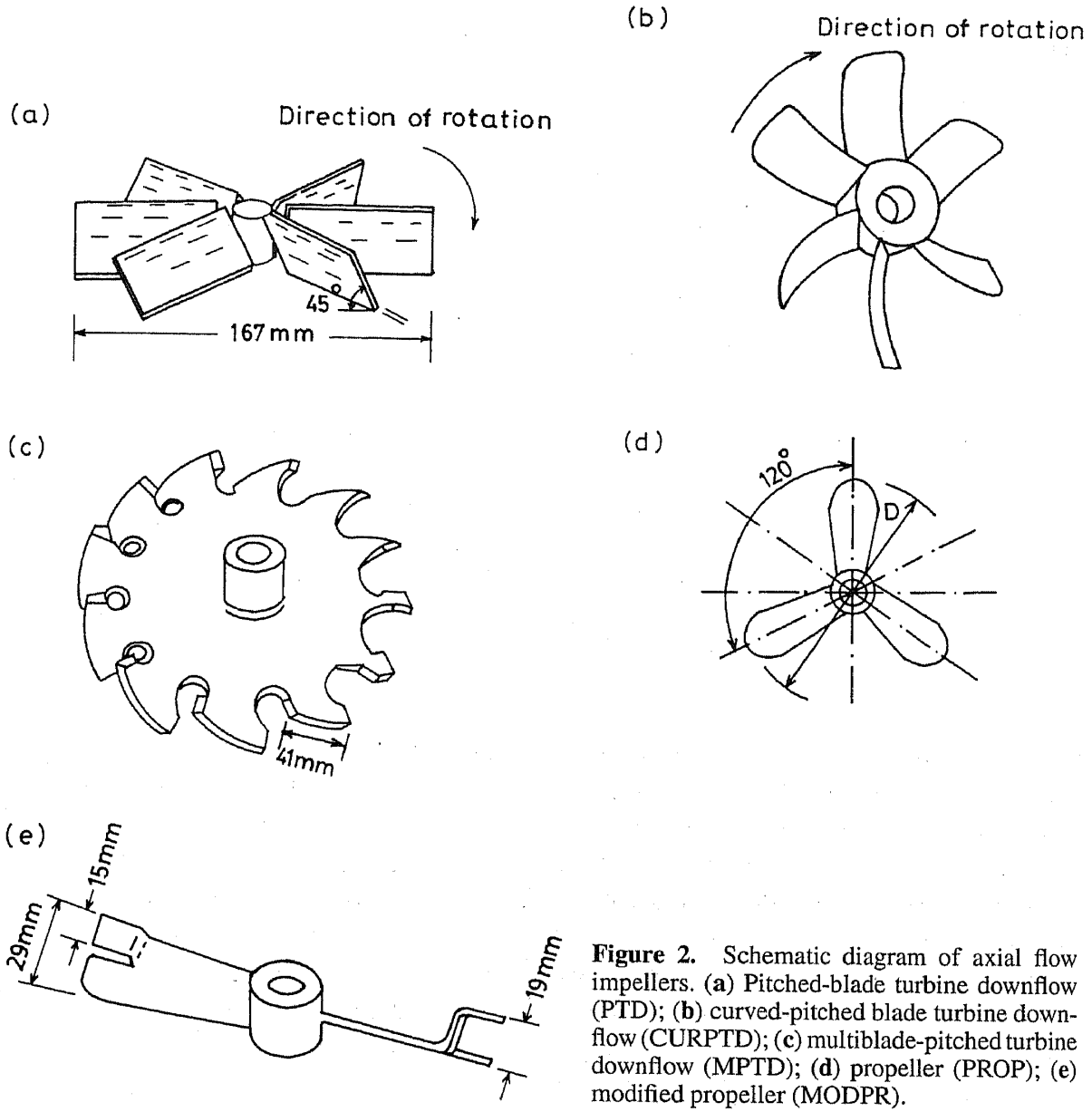

Figure 2. Schematic diagram of axial flow impellers. (**a**) Pitched-blade turbine downflow (PTD); (**b**) curved-pitched blade turbine downflow (CURPTD); (**c**) multiblade-pitched turbine downflow (MPTD); (**d**) propeller (PROP); (e) modified propeller (MODPR).

greater than the diameter. Both the vessels and the square tanks were made of transparent plexiglass. The outer square vessel was filled with water. All the impellers were made of stainless steel.

The impellers considered here are (i) pitched-blade downflow turbine (PTD), (ii) curved pitched downflow turbine (CURPTD), (iii) multiple pitched bladed downflow turbine (MPTD), (iv) propeller (PROP), (v) modified propeller (MODPR). These impellers have been shown schematically in figures 2a–e. The predicted values are compared with those of the experimental data for the above mentioned five impeller designs.

3. Mathematical formulation

A three-dimensional steady flow generated by an axial flow impeller in a cylindrical vessel with four equally spaced baffles was considered. Due to the presence of baffles at equal

Table 3. Source terms for the generalised equation.

Φ	Γ_{eff}	S_Φ
1	0	0
u	$\mu+\mu_t$	$C_D\left[\frac{1}{r}\frac{\partial}{\partial r}\left(r\Gamma_{\text{eff}}\frac{\partial u}{\partial r}\right)+\frac{\partial}{\partial z}\left(\Gamma_{\text{eff}}\frac{\partial v}{\partial r}\right)+\frac{1}{r}\frac{\partial}{\partial\theta}\left(\Gamma_{\text{eff}}\frac{\partial w}{\partial r}\right)-\frac{1}{r}\frac{\partial}{\partial\theta}\left(\Gamma_{\text{eff}}\frac{w}{r}\right)-\frac{2\Gamma_{\text{eff}}}{r^2}\frac{\partial w}{\partial\theta}-\frac{2\Gamma_{\text{eff}}u}{r^2}\right]-\frac{\partial p}{\partial r}-\frac{2}{3}\frac{\partial k}{\partial r}+\frac{w^2}{r}$
v	$\mu+\mu_t$	$C_D\left[\frac{1}{r}\frac{\partial}{\partial r}\left(\Gamma_{\text{eff}}\frac{\partial u}{\partial z}\right)+\frac{1}{r}\frac{\partial}{\partial\theta}\left(\Gamma_{\text{eff}}\frac{\partial w}{\partial z}\right)+\frac{\partial}{\partial z}\left(\Gamma_{\text{eff}}\frac{\partial v}{\partial z}\right)\right]-\frac{2}{3}\frac{\partial k}{\partial z}-\frac{\partial p}{\partial z}$
w	$\mu+\mu_t$	$C_D\left[\frac{1}{r}\frac{\partial}{\partial r}\left(\Gamma_{\text{eff}}\frac{\partial u}{\partial\theta}\right)+\frac{\partial}{\partial z}\left(\frac{\Gamma_{\text{eff}}}{r}\frac{\partial v}{\partial\theta}\right)+\frac{1}{r}\frac{\partial}{\partial\theta}\left(\frac{\Gamma_{\text{eff}}}{r}\frac{\partial w}{\partial\theta}\right)+\Gamma_{\text{eff}}\frac{\partial}{\partial r}\left(\frac{w}{r}\right)-\frac{1}{r}\frac{\partial}{\partial r}(\Gamma_{\text{eff}}w)+\frac{\Gamma_{\text{eff}}}{r^2}\frac{\partial u}{\partial\theta}+\frac{1}{r}\frac{\partial}{\partial\theta}\left(\frac{2\Gamma_{\text{eff}}u}{r}\right)\right]-\frac{2}{3}\frac{1}{r}\frac{\partial k}{\partial\theta}-\frac{1}{r}\frac{\partial p}{\partial\theta}-\frac{uw}{r}$
k	$\mu+\mu_t/\sigma_k$	$G-\epsilon$
ϵ	$\mu+\mu_t/\sigma_\epsilon$	$\frac{\epsilon}{k}(C_1G-C_2\epsilon)$, where $G=C_D\mu_t\left[2\left[\left(\frac{\partial u}{\partial r}\right)^2+\left(\frac{1}{r}\frac{\partial w}{\partial\theta}+\frac{u}{r}\right)^2+\left(\frac{\partial v}{\partial z}\right)^2\right]+\left(r\frac{\partial}{\partial r}\left(\frac{w}{r}\right)+\frac{1}{r}\frac{\partial v}{\partial\theta}\right)^2+\left(\frac{1}{r}\frac{\partial v}{\partial\theta}+\frac{\partial w}{\partial z}\right)^2+\left(\frac{\partial u}{\partial z}+\frac{\partial v}{\partial r}\right)^2\right]$, $\mu=\frac{\bar{\mu}}{C_D\rho U_{\text{tip}}}$, $\mu_t=\frac{k^2}{\epsilon}$

space intervals, flow was assumed to be periodic. Hence, a quadrant of the vessel was used for numerical simulation. The standard k-ϵ turbulent model was chosen for numerical simulation. The impeller was placed at $H/3$ from the vessel bottom. A cylindrical coordinate system was used with the origin located at the impeller centre and the angular position $\theta = 0$ was coincided with one of the baffle planes. For the sake of sign convention, the z coordinate below the impeller was taken as positive and that above the impeller as negative. The transport equation for a generalised variable Φ for an incompressible flow in nondimensional coordinate system was written as (Sahu *et al* 1998):

$$\frac{1}{r}\frac{\partial}{\partial r}(ur\Phi)+\frac{1}{r}\frac{\partial}{\partial\theta}(w\Phi)+\frac{\partial}{\partial z}(v\Phi)=\frac{1}{r}\frac{\partial}{\partial r}\left(r\Gamma_{\text{eff}}\frac{\partial\Phi}{\partial r}\right)+\frac{1}{r}\frac{\partial}{\partial\theta}\left(\frac{\Gamma_{\text{eff}}}{r}\frac{\partial\Phi}{\partial\theta}\right)+\frac{\partial}{\partial z}\left(\Gamma_{\text{eff}}\frac{\partial\Phi}{\partial z}\right)+S_\Phi. \tag{1}$$

The expressions for Γ_{eff} and S_Φ are given in table 3. The non-dimensional procedure was the same as in Sahu & Joshi (1995). The set of boundary condition for (1) is given as follows,

at $r = 0$ for $z \leq 0$ and all θ

$$u=\frac{\partial v}{\partial r}=w=\frac{\partial k}{\partial r}=\frac{\partial\epsilon}{\partial r}=0.0. \tag{2}$$

For $z < 0$, $r = r_s$, for all θ,

$$u=v=k=\epsilon=0;\ w=w_s,$$

at $r = 1$ for all z and θ,

$$u=v=w=k=\epsilon=0.0,$$

at $z = 2/3$ for all r and θ,

$$u = v = w = k = \epsilon = 0.0,$$

at $z = -4/3$ for all r and θ,

$$\frac{\partial u}{\partial z} = v = \frac{\partial w}{\partial z} = \frac{\partial k}{\partial z} = \frac{\partial \epsilon}{\partial z} = 0.0, \tag{3}$$

at $\theta = 0$ for all $r > r_b$ and z; $\theta = \pi/2$ for all $r > r_b$ and z,

$$u = v = w = k = \epsilon = 0.0.$$

In the impeller region, the boundary conditions for u, v, w and k were provided from the experimental data. As the velocity components (u, v, w) are provided in the impeller vicinity, it may be thought that the eddy viscosity coefficient is known (implicitly). Hence, giving either the values of k or ϵ, the other variable can be determined numerically. Therefore a guess value of ϵ was provided at the impeller region in the starting of the computation and was adjusted iteratively with the local values of the dissipation rate.

In case of high Reynolds number flows, it is a general practice to modify the no-slip condition by the introduction of the wall function (Launder & Spalding 1974). The wall function approach has several advantages: (i) It requires less computer time and storage, (ii) it allows the introduction of additional empirical information, and (iii) produces relatively accurate results with fewer node points in the near-wall region. Therefore, the implementation of the no-slip condition was done by setting the normal velocity to the wall to zero and the tangential velocity to the wall was specified by an empirical relation. In the present analysis, the logarithmic velocity variation has been used in the near-wall region for $y^+ > 30$.

$$\overline{U} = \overline{U}_r \ln(Ey^+)/\gamma, \tag{4}$$

$$\overline{\tau}_w = \rho \overline{U}_p C_D^{1/4} \overline{k}_p^{1/2} \gamma / \ln(Ey_p^+), \tag{5}$$

where $y_p^+ = \rho \overline{y} \overline{U}_r / \overline{\mu}$, γ is von Karman's constant, $\overline{U}_r$, is the friction velocity. The subscript p denotes the values of the variables at first node point near the wall. The value of the von Karman's constant γ is selected in the range of 0.41 ± 0.015 (Patel *et al* 1986). After modifying the no-slip condition for incorporating the wall function, it is also necessary to modify the turbulent kinetic energy k and the dissipation rate ϵ in the near-wall region.

The full implication of the assumption of logarithmic velocity profile can be realised, if (i) the shear stress in the near-wall region is uniform, (ii) the generation and dissipation of energy are in balance ($\overline{\tau}/\rho = C_D^{1/2} \overline{k} = \overline{U}_r^2$). These above mentioned assumptions demand that at the wall

$$\partial k/\partial y = 0, \epsilon = C_D^{3/4} k_p^{3/2}/y\gamma. \tag{6}$$

4. Numerical method of solution

To solve the set of elliptic partial differential equation (1) an efficient numerical algorithm should be used, which is numerically stable and accurate. Sahu & Joshi (1995)

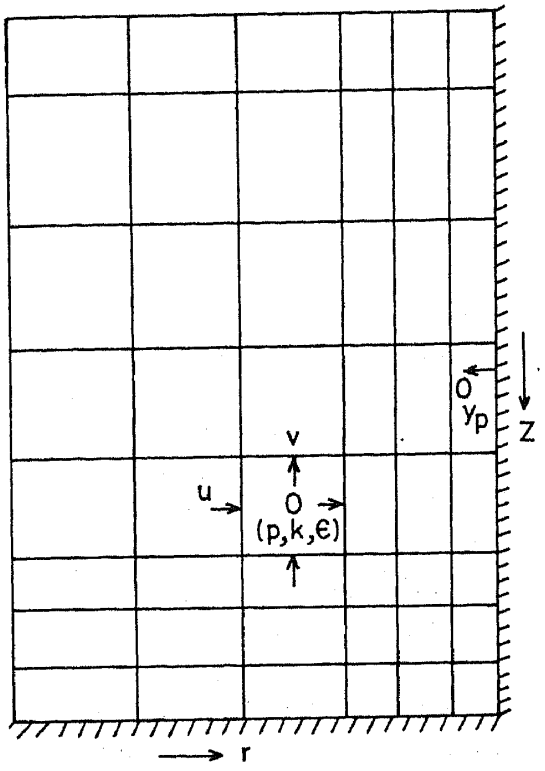

Figure 3. Distribution of non-uniform staggered grid system in r-z plane.

have discussed the pertinent details. A stable method implies that the discretisation of the convective and diffusive terms should be made in such a way that the coefficients of the dependent variables should satisfy the Scarborough criteria (Patankar 1980). In the present analysis, we have used three such numerically stable schemes: (i) Upwind scheme (UPS), (ii) hybrid scheme (HBS), (iii) power-law scheme (PLS). A detailed discussion on the advantages and disadvantages of the various schemes may be found elsewhere (Patankar 1980). A staggered grid system of control volume method has been used. The grid arrangements for the flow variables (2D) is shown in figure 3. This grid system has an advantage in solving the velocity field, since the pressure gradients are easy to evaluate and the velocities are conveniently located for the calculation of the convective fluxes. The pressure and the mean velocities are solved iteratively using the SIMPLE algorithm in 2D solution. In case of 3D simulation, it was observed that the rate of convergence of SIMPLE algorithm was very slow. Therefore, the SIMPLER algorithm was employed to solve the pressure and mean velocity equations iteratively.

Before discussing the solution technique for the set of algebraic equations for the flow variables, it would be appropriate to discuss the procedure for the inclusion of boundary conditions to these equations for the different flow variables. The gradient condition at the wall can be incorporated by equating the wall coefficient to zero. The incorporation of the wall function can be made in various ways: (i) Augmenting the μ_{eff} at the wall and taking tangential velocity at the wall to be zero (Dutta & Acharya 1993), (ii) equating the wall coefficient to be zero and augmenting the source term (Harvey & Greaves 1982), (iii) calculating the gradient of tangential velocity at the wall as $\partial\Phi/\partial y = U_r/\gamma y$ ($\Phi = u, v$) (Obi & Peric 1991; Elkaim *et al* 1993).

In the present analysis, it is found that the last approach takes less number of iterations for obtaining the converged solution as compared to the other two approaches. Moreover, the results obtained by the last two approaches are almost the same, whereas the results obtained by the first approach deviates slightly from the other two. As we have adopted an iterative process to obtain the solution, the algebraic equations for a given variable can be treated as linear. These linear equations have been solved iteratively using the Gauss–Seidel (GS) point-by-point method and the line-by-line method. The line-by-line method, also is known as ADI (Alternating Direction Implicit), was introduced by Peaceman & Rachford (1955). In the line-by-line method, the equations for the grid points along a chosen line would appear to be one-dimensional and are solved by the tridiagonal matrix algorithm (TDMA). The advantages and disadvantages of both the iterative processes for solving the algebraic equations have been discussed later. Due to the iterative nature of the solution algorithm the algebraic equations for a given variable need not be taken to complete convergence. It will be shown later that an excessive amount of effort on solving the algebraic equations that are based on only tentative coefficients is an unnecessary waste of computer time. Further, to achieve a better convergence, the mean velocities, the pressure corrections and the turbulent quantities need to be under-relaxed with the suitable values of the under-relaxation parameters. Furthermore, the guess values for the flow variables should also be chosen properly for obtaining a converged solution. A detailed discussion on these points has been given later. The computations for a two-dimensional system have been carried out in T808 transputer with PC 386. Three-dimensional computations were carried out on a Pentium PC. The iterative process is terminated when the mass source residue over each control volume is less than 10^{-4} and the residues for momentum, turbulent kinetic energy and dissipation rate are less than 10^{-5}. It has been found that when mass residue is less than 5×10^{-4}, the residual correction for the momentum and turbulence variables are automatically satisfied.

5. Results and discussion

Before presenting the numerically predicted values for the flow variables at different axial positions and their comparison with experimental data, it is worth discussing the following few points which are very important for numerical calculations: (i) Comparison of the different numerical schemes, (ii) effects of internal iteration on the rate of convergence and the iterative processes for solving the algebraic equations, (iii) effects of the grid size (global and near-wall region), (iv) effects of the under-relaxation parameters on the rate of convergence, (v) effects of guess values of the variables on the rate of convergence, and (vi) effects of the model parameters on the solution. Sahu & Joshi (1995) have investigated this subject in detail.

5.1 *Comparison of different numerical schemes (2D)*

Effects of various numerical schemes on the predicted values of the flow characteristics have been shown in figure 4 (Sahu & Joshi 1995). It is observed that the predictions of the flow characteristics by the hybrid and power-law schemes are almost the same, whereas the

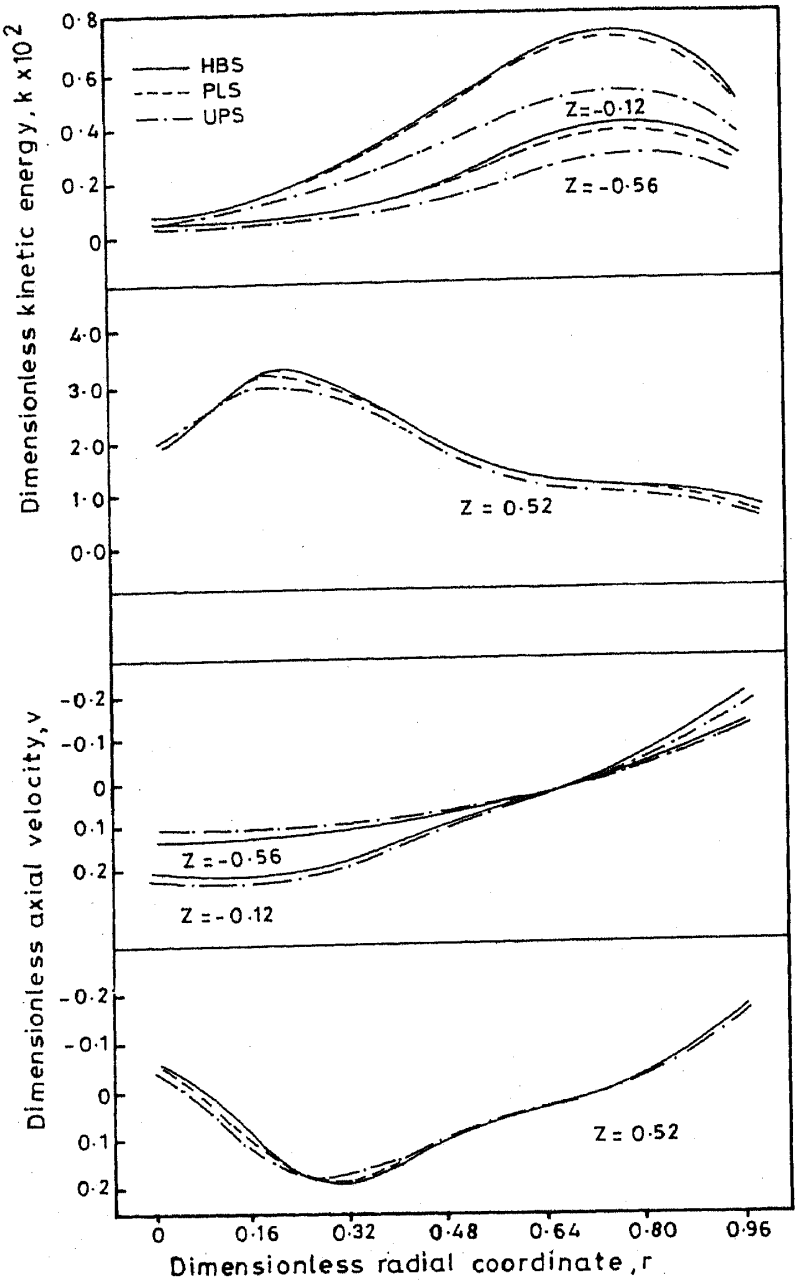

Figure 4. Effects of various numerical schemes on the axial velocity and turbulent kinetic energy distribution at different axial positions.

solution obtained by the upwind scheme differs substantially from the other two schemes. Further, the rate of convergence of the power-law scheme is faster than that of the hybrid scheme. However, the upwind scheme converges at a faster rate than the power law scheme (figure 5). The time taken by the upwind, hybrid and power-law schemes per iteration under identical conditions is 4, 4.14 and 4.8 s respectively. The total time consumed by the upwind, hybrid and power-law schemes to obtain the converged solution under identical conditions is 24, 31 and 33 min respectively. Although the upwind scheme takes much less time compared to the other two schemes, it may not be accepted for the numerical simulation of an axial flow impeller due to the underprediction of the values of the flow variables. Further, there are no significant differences in the computational time between

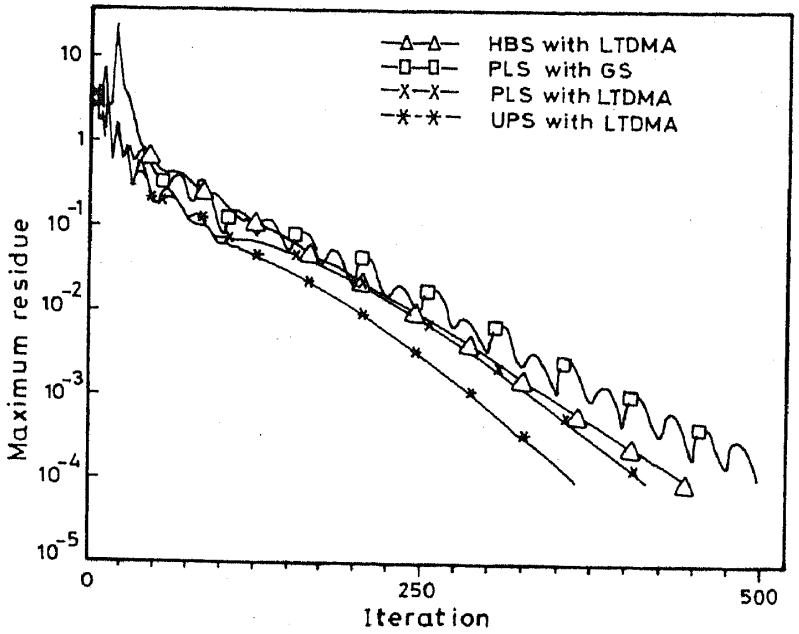

Figure 5. Effects of various schemes and iterative processes on the rate of convergence.

the power-law and the hybrid schemes. Therefore, for the robustness of the algorithm, the power-law scheme has been used.

5.2 *Effects of internal iteration on the rate of convergence (2D)*

For an iterative process, it is normal practice that two or three iterations are used for solving the algebraic equations for u, v, k, and ϵ and the number of iterations used for pressure correction equations is four to five times that of the said variables with the line-by-line TDMA method. It may be pointed out here that the above practice does not yield a better convergence (table 4). As the coefficients of the velocity variables are influenced by the eddy viscosity, the solution of the k and ϵ equations should be iterated more times than the pressure correction equation. Further, an excessive number of internal iterations for k and ϵ also does not enhance the rate of convergence of the solution. It may be remarked that a more accurate solution for the pressure correction equation slows down the convergence. Similar observations have also been made by Patankar (1980). It has been observed that, besides the iterative process, the under-relaxation parameters, initial guess values etc., the

Table 4. Effects of internal iterations on the rate of convergence ($C_D = 0.05$, $C_1 = 1.44$, $C_2 = 1.92$, $\sigma_k = 1$, $\sigma_\epsilon = 1.3$, $\gamma = 1$).

Pressure correction equation	Velocity equations	Turbulent kinetic energy equation	Turbulent energy dissipation rate equation	Iterations
4	3	4	4	510
6	3	4	4	518
4	3	7	4	320
4	3	10	4	320
4	3	4	7	544
4	2	7	4	320

eddy viscosity calculations at control volume faces also have significant effect on the rate of convergence. It is generally accepted that, due to the rapid variation of eddy viscosity in the spatial direction, at control volume faces, the values of the variables are calculated by using the harmonic mean instead of the arithmetic mean. However, in the present study, it is found that this practice sometimes yields a divergent solution. This may be due to the small magnitudes of the k and ϵ variables in the upper part of the vessel, which augments the round-off error. Finally, it will be worth mentioning the advantages and the disadvantages of the Gauss–Seidel point-by-point and the line-by-line TDMA (LTDMA) iterative processes. It is found that the Gauss–Seidel method (GS) takes more iterations for obtaining a converged solution as compared to the line-by-line TDMA method when the algebraic equations are obtained by using the power-law scheme (figure 5). Further, under identical conditions the Gauss–Seidel iterative process produces an oscillating solution. The time taken for completing one iteration by using the Gauss–Seidel method and the line-by-line TDMA method is about 4.28 and 4.8 s respectively. However, the total time required to obtain a converged solution with the help of the Gauss–Seidel method is higher than that of the line-by-line TDMA method. Hence, the line-by-line TDMA method has been used for all the purposes. The oscillating behaviour of the Gauss–Seidel method may be overcome by increasing the internal iterations of the variables, consequently there is a further increase in the computational time. From these observations, one may conclude that a better iterative process for solving the algebraic equations may reduce the computational cost.

5.3 *Effects of grid sizes (2D)*

The grid sizes taken to show the grid independence of a solution are of two types, the effects of the near-wall grid size and the overall grid size. It may be observed from figure 6 that the introduction of a fine grid system in the near-wall region does have an effect in the near-wall region, as well as in the bulk region. The only difficulty is that, with an increase in the grid density near the wall, the computational time increases. Approximately, an increase of one grid point near the wall region results in an increase in total number of iterations by fifty with the same guess values and the under-relaxation parameters. It is very interesting to note that the predicted value of the turbulent kinetic energy near the wall has a sudden jump when the solution is obtained by using a uniform grid size (figure 6). This behaviour is not observed with the introduction of a fine grid size near the wall region. The behaviour of the predicted values of k for a fine grid size is in conformity with experimental data. It may be pointed out that, below the impeller region, one subdivision of near-wall control volume gives a grid independent solution (figures 6a,c), whereas in the upper part of the vessel three to four subdivisions are necessary to obtain a grid independent solution (figure 6). This variation may be related to the small magnitude of the turbulent kinetic energy predicted in this region. Does this imply that due to the low values of the turbulent kinetic energy, the logarithm variation of the tangential velocity profile to the wall is confined to a very thin layer? In the present calculation, three node points have been introduced in the near-wall region. To study the effects of overall grid size on the flow variables, the grid sizes chosen are 28×19, 14×44, 28×33 and 35×41. It is of interest to note that the lower number of grid points in the axial and radial directions underpredict

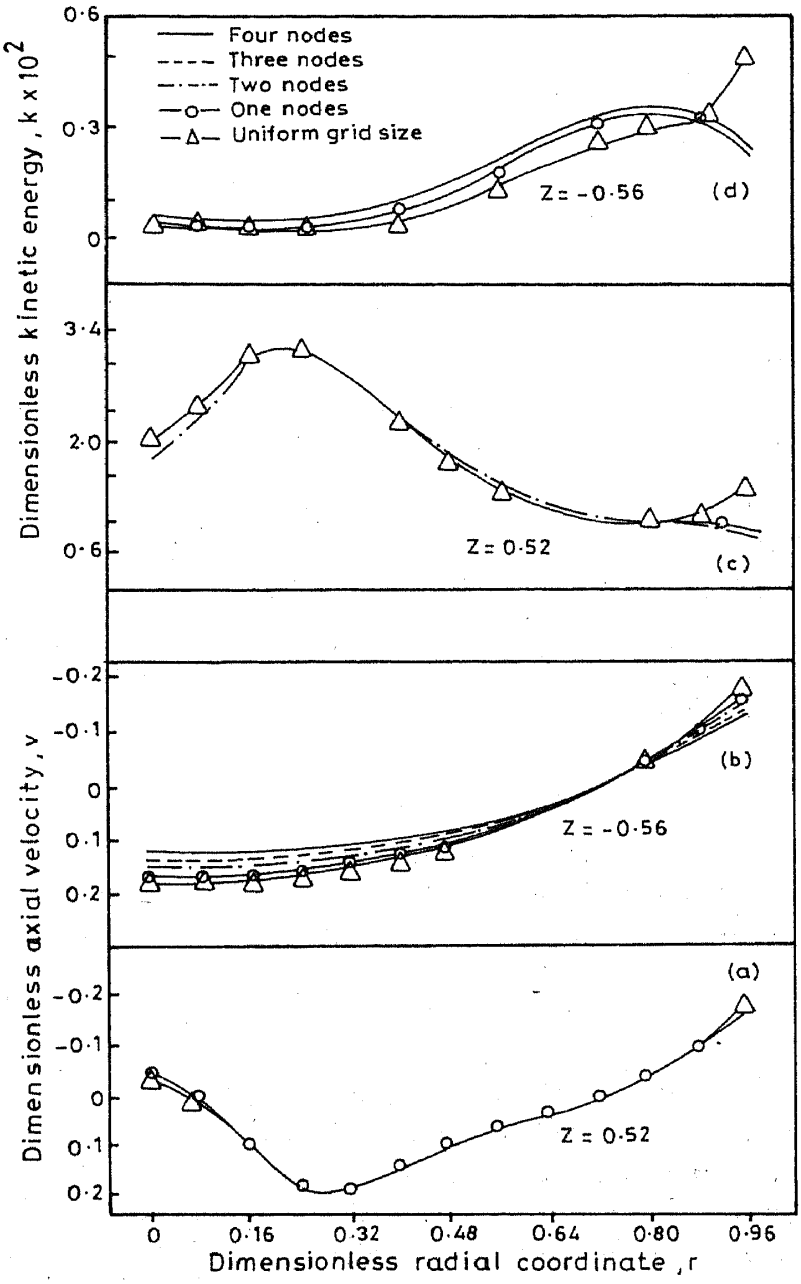

Figure 6. Effects of near-wall grid points on the axial velocity and turbulent kinetic energy at different axial positions.

the radial velocity and the turbulent kinetic energy and overpredict the axial velocity. It may be remarked that the variation in the magnitude of the axial velocity which has been predicted by using the grid sizes 14×44 and 28×33 is about 15%. It is also observed that the difference in the results obtained by grid sizes 28×33 and 35×41 is almost negligible. Hence, to conserve computational time, in the present study, a grid density of 28×33 has been used. Although the flow characteristics are independent of the grid size for a grid density of 28×33, the numerical predictions of the average dissipation rate (ϵ_{av}) (table 3) converge to a limiting value for the large grid system, particularly in the axial direction. The variation of the average dissipation rate with various grid densities has been shown in table 5. An analysis of the numerical data for ϵ_{av} suggests that for large grid sizes, its value

Table 5. Effect of grid size on average turbulent energy dissipation rate ($C_D = 0.05$, $C_1 = 1.44$, $C_2 = 1.92$, $\sigma_k = 1$, $\sigma_\epsilon = 1.3$, $\gamma = 0.42$).

Grid size	35 × 41	21 × 41	21 × 44	21 × 26	28 × 26	28 × 44	28 × 33	35 × 56
$\epsilon_{av} \times 10^3$	2.50	2.43	2.40	2.60	2.66	2.46	2.56	2.42
Iteration	512	381	373	360	431	450	440	504

approaches a limiting value. The variation in the value of ϵ_{av} for the grid systems 28 × 33 and 35 × 56 is about 5%, whereas its variation for grid systems 28 × 19 and 35 × 56 is approximately 16%.

5.4 *Effects of the under-relaxation parameters on the rate of convergence (2D)*

It has been shown by Peric *et al* (1987) that a nearly optimum convergence is found for the SIMPLE algorithm for $\alpha_p = 1 - \alpha_u$. However, in the present study, it has been observed that along with the under-relaxation parameters for the pressure and the velocities, the under-relaxation parameters for k and ϵ and the eddy viscosity are also vital to obtain a converged solution. With the suitable guess values for the flow variables, it may be noticed from table 6 that for the values of

$$\alpha_p = 0.6, \alpha_u = 0.4, \alpha_k = 0.1, \alpha_\epsilon = 0.25, \alpha_e = 0.5,$$

an optimum convergence can be achieved to obtain solution, where $\alpha_p, \alpha_u, \alpha_k, \alpha_\epsilon, \alpha_e$ are the under-relaxation parameters for the pressure, velocities, turbulent kinetic energy, turbulent energy dissipation rate and eddy viscosity calculations respectively.

5.5 *Effects of guess values of the variables on the rate of convergence (2D)*

The effects of the initial guess values on the rate of convergence has been shown in table 7. It is interesting to note that the guess values for u and v practically have no influence on the rate of convergence. However, the rate of convergence of the iterative process primarily depends upon the guess value of k and ϵ. It is very difficult to establish any mathematical relation between the guess values of k and ϵ which yield an optimum rate of convergence. However, an analysis of the numerical data of table 7 suggests that a proper choice for the

Table 6. Effects of the under-relaxation parameters on the rate of convergence with a given initial guess solution. Parameter values are the same as in table 4.

α_p	α_u	α_k	α_ϵ	α_e	Iterations
0.25	0.5	0.1	0.5	0.4	483
0.25	0.5	0.1	0.15	0.4	498
0.25	0.75	0.1	0.25	0.4	337
0.5	0.5	0.1	0.25	0.4	300
0.6	0.4	0.1	0.25	0.4	294
0.6	0.4	0.1	0.25	0.5	294
0.25	0.5	0.15	0.25	0.4	570

Table 7. Effects of initial guess values of the flow variables (u, v, k, ϵ) on the rate of convergence for a given set of under-relaxation parameters ($\alpha_p = 0.6$, $\alpha_u = 0.4$, $\alpha_k = 0.1$, $\alpha_\epsilon = 0.25$, $\alpha_e = 0.4$). Parameter values are the same as in table 4.

u	v	k	ϵ	Iterations
0.025	−0.021	0.015	0.005	294
0.0025	−0.021	0.015	0.005	294
0.025	−0.051	0.015	0.005	294
0.025	−0.021	0.010	0.005	288
0.025	−0.021	0.005	0.005	271
0.025	−0.021	0.015	0.05	408
0.025	−0.021	0.0025	0.005	608
0.025	−0.021	0.002	0.002	681
0.025	−0.021	0.005	0.05	Diverged

guess values of k and ϵ may be found based on the information of ϵ_{av} (table 8). It is found that, in the numerical calculation of the flow characteristics, for all the impellers which have been considered in the present study, the guess values of ϵ is approximately three to four times that of average dissipation rate and the k value may be of the same order as the value of ϵ. It is clear from table 7 that a bad guess value for k and ϵ not only slows down the rate of convergence but also yields a divergent solution. It may be remarked here that a good starting value for k and ϵ can drastically reduce the total number of iterations for obtaining a converged solution, which ultimately reduces the computer time. In the present analysis, to start with, we have provided uniform profiles for all the flow variables. However, non-uniform profiles for the flow variables may result in rapid convergence, which has not been attempted here.

5.6 *Effects of under-relaxation, initial guess values, internal iterations and grid size (3D)*

It was observed that the under-relaxation parameters for flow variables should be adjusted very carefully for obtaining a converged solution. Sahu *et al* (1998) have investigated this subject in detail. With the increase of grid size, a careful selection of under-relaxation parameters was needed for the calculation of axial and tangential velocities. To begin with the iterative process, the values of the under-relaxation parameters for axial and tangential components were taken as 0.05 and 0.12 respectively. If these under-relaxation parameters were retained during computation, the iterative process became very slow. To overcome this difficulty, the magnitude of the initial set of under-relaxation parameters

Table 8. Comparison between the predicted and the experimental values of the average turbulent energy dissipation rate $\epsilon_{av} \times 10^3$ ($C_1 = 1.44$, $C_2 = 1.92$, $\sigma_k = 1$, $\sigma_\epsilon = 1.3$, $\gamma = 0.42$).

Impellers	PTD	CURPTD	MPTD	PROP	MODPR
Experimental	3.16	3.74	2.28	1.67	0.87
$C_D = 0.05$	4.07	4.45	1.68	1.30	0.79
$C_D = 0.09$	5.03	5.18	1.98	1.55	0.90

was increased at regular intervals depending on the magnitude of the source term or the total number of iterations needed, till the set of parameters attained an optimal value for which convergence was obtained with optimum CPU time. It was observed that these optimal values of under-relaxation parameters were 0.45, 0.35, 0.45, 0.25, and 0.30 for radial, axial, tangential velocities, turbulent kinetic energy and turbulent energy dissipation rate respectively. For pressure equation, a fixed relaxation parameter of 0.75 was used. For two-dimensional flow, Sahu & Joshi (1995) observed that the relation between the relaxation parameters of velocities and pressure correction may be expressed by a simple equation $\alpha_u = 1 - \alpha_p$. Similar observations had also been made by Peric *et al* (1987). However, for three-dimensional simulation, no such relation could be established (Sahu *et al* 1998). In the case of two-dimensional flow, the relaxation parameters for axial and radial velocities were the same, whereas for three-dimensional flow they were different for different velocity components. It was seen that, in the two-dimensional analysis, initial guess values of k and ϵ had a great influence on the success of the iterative process. Similar observations were also made for three-dimensional analysis. The internal iterations required for the solution of algebraic equations for different variables are different. For velocities, six internal iterations were sufficient to obtain a converged solution. However, for the turbulent kinetic energy, a minimum of 15–20 internal iterations were required and approximately 10 internal iterations were needed for the turbulent energy dissipation rate equation. Although a fixed number of internal iterations were used for the above mentioned variables, for pressure and pressure correction equations, a different procedure was adopted to ensure convergence. To begin with, the internal iteration for pressure and pressure correction equations were taken as two and four respectively. As the iterative process progressed, these numbers were increased to fifteen to expedite the convergence. Normally, the first increment in the number of internal iteration was given after fifty iterations. Later, after an interval of ten iterations, the internal iterations for pressure and pressure correction equations were incremented.

In the literature, different authors have studied the effects of grid size and recommended different types of grid combination (Bakker & Van den Akker 1994; Fokema *et al* 1994). The effect of grid size for a 2D system was described in the previous section. In 3D simulations it was observed (Sahu *et al* 1998) that a grid size of $37 \times 15 \times 40$ (r, θ, z) yielded a grid-independent solution.

5.7 *Comparison between 2D and 3D predictions*

In the published literature, for the sake of simplicity, various authors (Harvey & Greaves 1982 ; Sahu & Joshi 1995) used two dimensional k-ϵ turbulent models to simulate the stirred baffled vessel. Therefore, it was pertinent to give a detailed comparison between experimental data and predicted values which were obtained by employing two dimensional and three-dimensional models for evaluating their efficiencies. This exercise has been provided by Sahu *et al* (1998). It was observed that the predicted three-dimensional radial velocity profile at $z = 0.586$ agreed well with the experimental data in the range $r \leq 0.6$, except close to the axis (figure 7a). The predicted two-dimensional values were higher in this region. Beyond this region, the predicted values obtained by both the models were almost the same and close to the experimental values (figure 7a). At $z = 0.36$

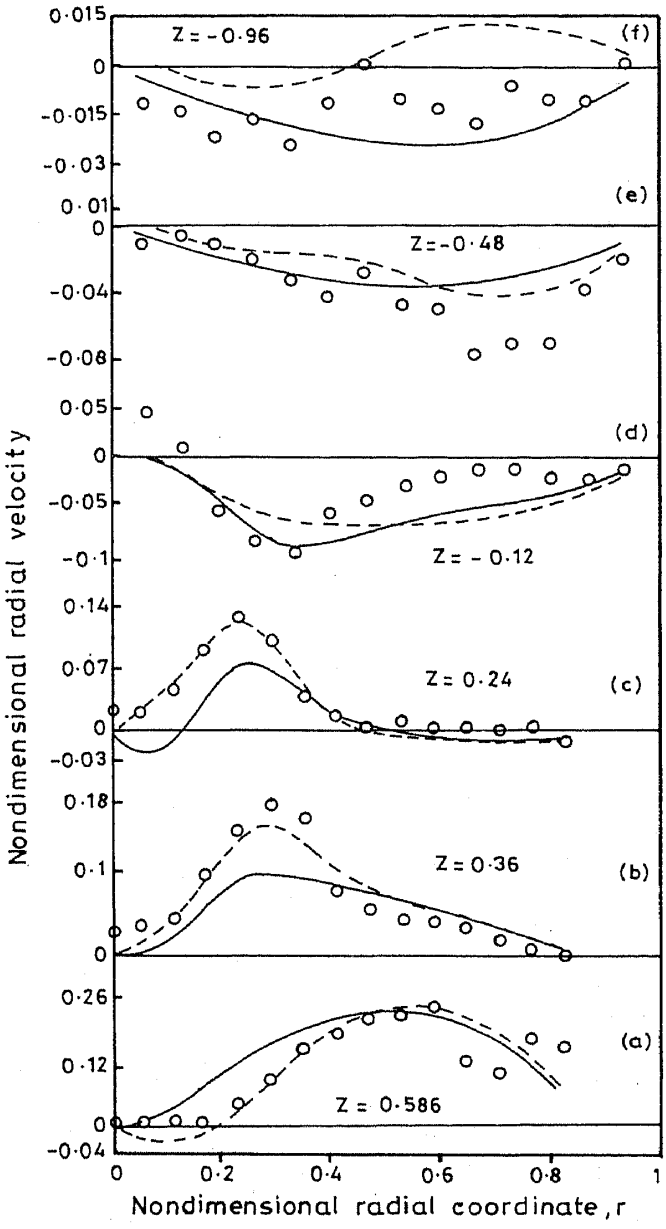

Figure 7. Comparison of two- and three-dimensional predicted values of radial velocity with experimental value for PTD. (o, experimental; —, 2D; - - -, 3D.)

(figure 7b) and $z = 0.24$ (figure 7c) the three-dimensional predictions agreed well with the experimental data, whereas two-dimensional solution agreement was good only when $r > 0.4$. Above the impeller, two dimensional predictions of radial velocity were seen to be better than the three-dimensional prediction ($z = -0.12, -0.96$) except at $z = -0.48$ (figures 7d–f). The predicted two-dimensional and three-dimensional axial velocity profiles below the impeller were almost the same for $r \geq 0.375$ and their comparisons with experimental data were also very good (figures 8a–c), whereas for $r < 0.375$ the predicted three-dimensional solution was very good. It was noticed that as one moved towards the bottom of the vessel from the impeller, the difference between the two-dimensional prediction and experimental data widened near the axis (figures 8a–c). This disagreement might be due to the omission of the tangential velocity component in the two-dimensional prediction. Above the impeller ($z = -0.12, -0.48, -0.96$) the three-dimensional prediction was in better agreement with experimental data as compared to the two-dimensional

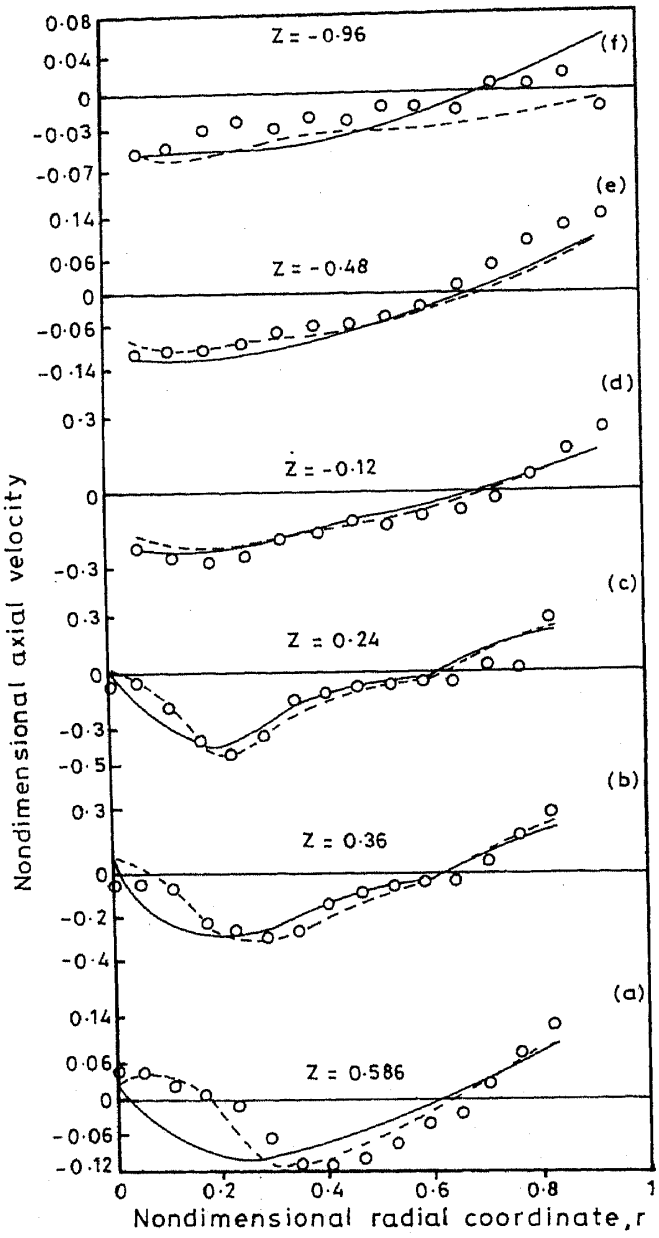

Figure 8. Comparison of two- and three-dimensional predicted values of axial velocity with experimental value for PTD. (o, experimental; —, 2D; - - -, 3D.)

prediction (figures 8d–f). An important aspect of the behaviour of the flow phenomena above the impeller was that the experimentally observed secondary circulation (figure 8f), was accurately predicted by the three-dimensional model. However, the two-dimensional model failed to demonstrate this behaviour, even close to the tank surface. This observation clearly showed the shortcoming of the two-dimensional prediction. The turbulent kinetic energy predicted by two-dimensional and three-dimensional models was in very good agreement with experimental data at $z = 0.24$ for $r > 0.4$ (figure 9c). As one moved towards the bottom of the vessel, three-dimensional models yielded better agreement with the experimental data as compared to the two-dimensional ones (figures 9a–c). Near the axis the predicted value of k with the two-dimensional model was found to be much higher than the experimental data (figures 9a–c) as compared with the three-dimensional prediction. Above the impeller ($z = -0.12, -0.48, -0.96$) the experimental data for turbulent kinetic

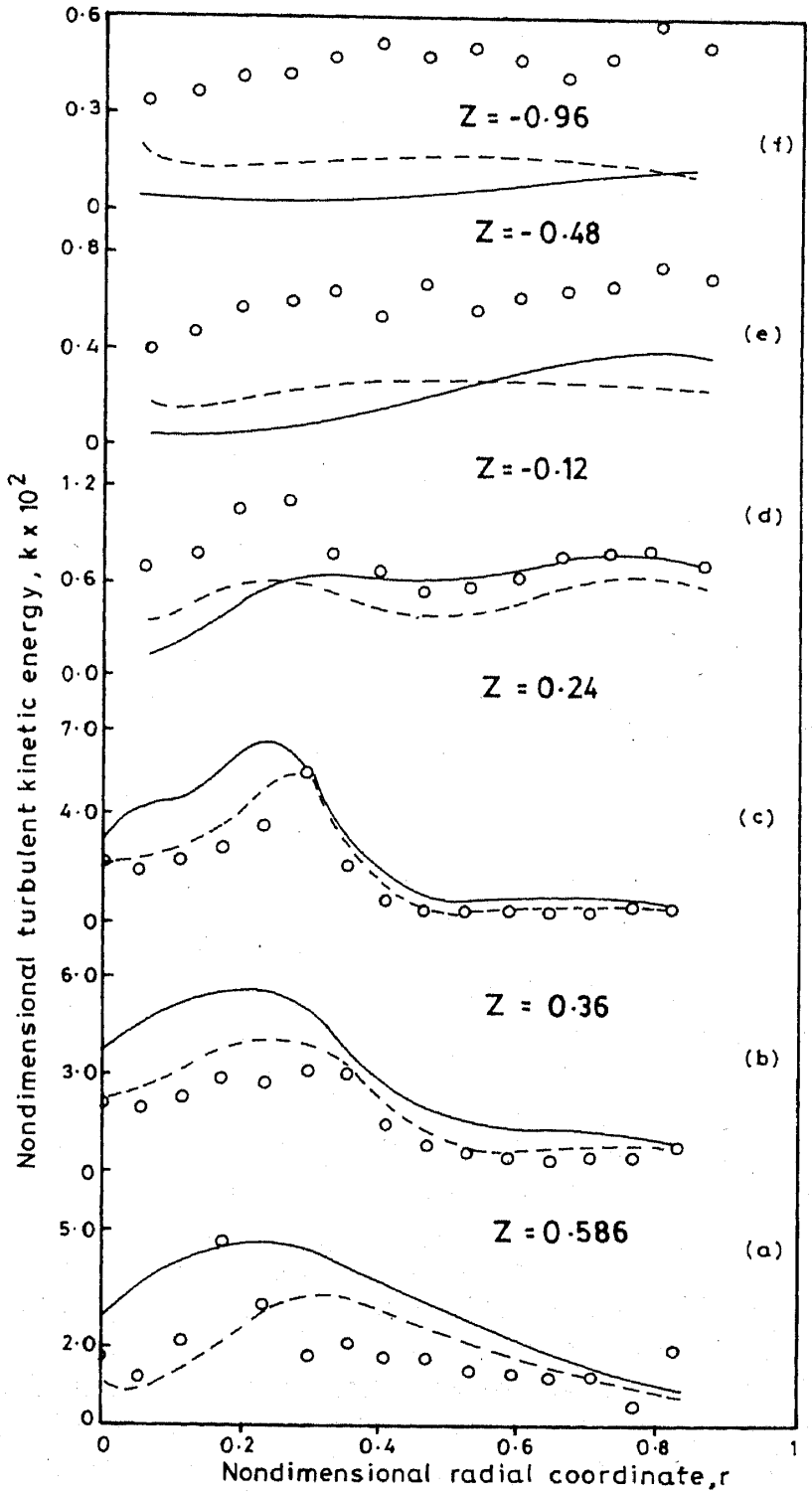

Figure 9. Comparison of two-and three-dimensional predicted values of turbulent kinetic energy for PTD. (o, experimental; —, 2D; - - -, 3D.)

energy was very much away from the two-dimensional as well as the three-dimensional predictions (figures 9d–f). However, it can be seen from figures 9e and f that the distribution of the turbulent kinetic energy was greater even in the case of three-dimensional prediction. It was also noticed that, below the impeller, the rate of reduction in the value of the turbulent kinetic energy within the region $r < 0.4$ for two-dimensional model was slower than that of three-dimensional model (figures 9a–c). This variation further signified the shortcoming of the two-dimensional model. All these above mentioned observations indicated that the two-dimensional model predictions were not good enough to give the details of the flow phenomena. Therefore, for better simulation, a three-dimensional model can be said to be desirable.

5.8 *Effect of model parameter*

Although Sahu & Joshi (1995) discussed the effects of model parameters on the flow characteristics in detail, in the study of Sahu *et al* (1998), a further elaboration was provided in view of the three-dimensional analysis and zonal modelling. Further, the success of the zonal modelling totally depended on the selection of model parameter values in different zones. This selection was possible only by knowing the variation of the flow characteristics in the entire vessel with respect to the turbulent model parameters.

5.9 *Zonal modelling*

Sahu *et al* (1998) have given the pertinent details of the zonal modelling. To start with, the entire flow domain was divided horizontally into two regions at the impeller centre plane and two sets of parameters were selected for each region. It was observed that the variation of the flow characteristics in one region did not significantly affect the flow characteristics in the other. This observation made it clear that, by dividing the flow domain into several zones, better agreement between the experimental and the predicted values could be obtained. Therefore, it was decided to divide the r-z flow domain into several sub domains. The parameter values were selected for each subdomain by the trial and error method. Each subdomain may be called a zone. To maintain the continuity of solution between the two neighbouring zones, the spline interpolation method was used. In this process, the parameter values did not change with respect to the angular position. To demonstrate the usefulness of the zonal modelling, the predicted flow characteristics were compared with the experimental data and predictions using the standard set of turbulent parameters. For the sake of brevity, the predicted results obtained by the zonal modelling will henceforth be called Z-P and by standard set of turbulent parameter will be termed S-P. The turbulent parameter values for zonal modelling have been shown in table 9. The values of these parameters have been selected based on their effects on flow characteristics to get good agreement between predicted and experimental values. Looking at the parameter values, at present, it has not been possible to present a general expression for the variation of parameter values. However, it may be remarked that the change of values of C_2 below the impeller is in accordance with Rodi (1993), who modified the values of C_2 for an axisymmetric jet flow in terms of dimensionless jet width, maximum velocity difference and gradients of maximum velocity. The values of C_2 obtained using the expression is less

Table 9. Turbulence model parameters for zonal modelling.

	r							
z	0	0.2	0.3	0.5	0.55	0.85	0.97	1.0
C_D								
0.667	0.25	0.25	0.05	0.050	0.050	0.05	0.09	0.09
0.567	0.25	0.25	0.05	0.050	0.050	0.05	0.09	0.09
0.267	0.09	0.09	0.05	0.050	0.050	0.05	0.09	0.09
0.067	0.09	0.09	0.09	0.090	0.090	0.09	0.09	0.09
−0.133	0.09	0.09	0.09	0.090	0.090	0.09	0.09	0.09
−0.333	0.09	0.09	0.09	0.090	0.090	0.09	0.09	0.09
−0.533	0.09	0.09	0.09	0.090	0.090	0.09	0.09	0.09
−0.733	0.09	0.09	0.09	0.090	0.090	0.09	0.09	0.09
−0.933	0.07	0.07	0.07	0.100	0.100	0.07	0.07	0.07
−1.133	0.05	0.05	0.05	0.125	0.125	0.05	0.05	0.05
−1.333	0.04	0.04	0.04	0.125	0.125	0.04	0.04	0.04
C_1								
0.667	1.440	1.440	1.440	1.440	1.440	1.440	1.440	1.440
0.567	1.440	1.440	1.440	1.440	1.440	1.440	1.440	1.440
0.267	1.440	1.440	1.400	1.400	1.440	1.440	1.440	1.440
0.067	1.440	1.440	1.440	1.440	1.000	1.000	1.000	1.000
−0.133	1.440	1.440	1.440	1.440	1.000	1.000	1.000	1.000
−0.333	1.440	1.440	1.440	1.440	1.000	1.000	1.000	1.000
−0.533	1.144	1.144	1.144	1.144	1.440	1.440	1.440	1.440
−0.733	1.144	1.144	1.144	1.144	1.440	1.440	1.440	1.440
−0.933	1.144	1.144	1.144	1.144	1.440	1.440	1.440	1.440
−1.133	1.144	1.144	1.144	1.144	1.440	1.440	1.440	1.440
−1.333	1.144	1.144	1.144	1.144	1.440	1.440	1.440	1.440
C_2								
0.667	1.920	1.920	1.500	1.500	1.500	1.500	1.500	1.500
0.567	1.920	1.920	1.500	1.500	1.500	1.500	1.500	1.500
0.267	1.920	1.920	1.500	1.500	1.500	1.500	1.500	1.500
0.067	1.920	1.920	1.620	1.620	1.620	1.620	1.620	1.620
−0.133	1.920	1.920	1.920	1.920	1.920	2.220	2.220	2.220
−0.333	1.920	1.920	1.920	1.920	1.920	2.220	2.220	2.220
−0.533	2.100	2.100	1.920	1.920	2.200	2.200	2.200	2.200
−0.733	2.300	2.300	1.920	1.920	2.500	2.500	2.500	2.500
−0.933	2.400	2.400	1.920	1.920	2.400	2.400	2.400	2.400
−1.133	2.500	2.500	1.920	1.920	2.600	2.600	2.600	2.600
−1.333	2.600	2.600	1.920	1.920	2.700	2.700	2.700	2.700

than the standard value. The impeller stream of the pitched blade turbine can be considered as jet flow and the values used for the present calculation are also less than the standard value, which confirms the observation of Rodi (1993). It may be observed in figures 10b and c that the predicted radial velocity profiles with Z-P at $z = -0.24$ and $z = 0.36$ were in excellent agreement with the experimental data. The same could not be said about the predicted result with S-P. Particularly, the peak values were not predicted accurately with S-P. Further, it was found that in the range $0.6 < r < 0.8$, the predicted profiles with Z-P merged with the experimental data which was not true for S-P. At $z = 0.586$, it was seen that the predicted radial velocity profiles with S-P and Z-P (figure 10) were almost the same and in good agreement with the experimental data for $r < 0.6$. It was also observed that the predicted axial velocity with Z-P at this location was in better agreement with the

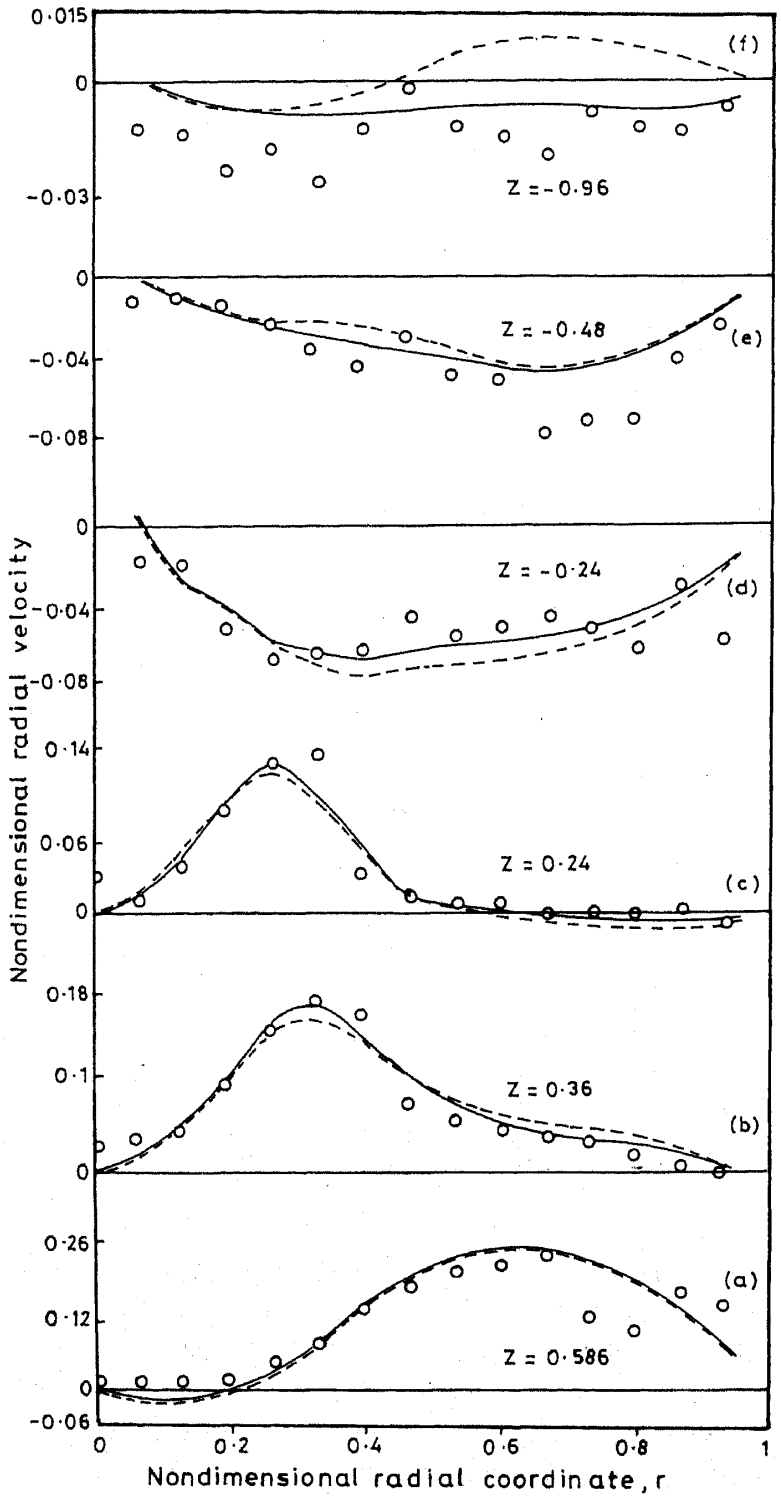

Figure 10. Comparison of predicted values of radial velocity with experimental value for PTD. (o, experimental; —, zonal; - - -, standard.)

experimental data as compared to the prediction of S-P. A similar remark could also be made for the prediction of tangential velocity and turbulent kinetic energy. From the above discussion, it is clear that zonal modelling improved the predictions below the impeller. From the literature review, it was seen that the main region of disagreement between the experimental and the predicted values was above the impeller. Therefore, detailed comparison was needed between the predictions of Z-P and the experimental data above the impeller. It was seen that at $z = 0.24$ the predicted radial velocity profile with Z-P was in better agreement with experimental data as compared to the predicted profile with S-P (figure 10). Excellent agreement between the experimental data and Z-P prediction was also observed for axial velocity profile at this location. At $z = -0.96$ the predicted radial velocity with Z-P were seen to be closer to the experimental data (figure 10). The predicted radial velocity profile (figure 10) at this position with S-P behaved in the opposite manner as compared to the experimental data. The near-wall discrepancy might be due to the wall boundary condition. From the above discussion, it is clear that the introduction of zonal modelling improves the predicted flow characteristic in the entire vessel. Further, by tuning the model parameters and employing zonal modelling the efficiency of the turbulent k-ϵ model could be enhanced for the simulation of flow in stirred vessels.

The variation in flow characteristics due to zonal modelling may be explained in terms of eddy viscosity. The parameter C_2 appears in the sink term (table 3), i.e. the term by which the dissipated energy is converted to heat. As C_2 decreases, it causes a decrease in energy dissipation rate. As a result, there is a decrease in the turbulent kinetic energy. The overall effect of the changes in ϵ and k causes a decrease in eddy viscosity and increase in velocity gradients. Opposite behaviour is observed with the decrease in C_1 since it is the coefficient of generation term. It is also well known that lowering the value of C_D decreases the eddy viscosity.

It was thought desirable to use the technique of zonal modelling for four other designs of axial flow impellers. The optimised sizes of zones and the corresponding parameters were maintained while simulating the other impeller designs. Excellent agreement was observed between the predictions of zonal modelling and experimental data for all the three components of the mean velocity and the turbulent kinetic energy.

6. Conclusion

The turbulent flow generated by various axial flow impellers was measured at several axial locations using LDA. The comparison of three numerical schemes shows that the power-law scheme is more robust and accurate as compared to the hybrid and upwind schemes. With the suitable combination of guess values of the variables and the under-relaxation parameters, the rate of convergence of the iterative process can be enhanced. The parametric effect study has shown that it is difficult to obtain a single set of parameters which can predict all the flow characteristics in close agreement with experimental data. Therefore, the concept of zonal modelling was introduced. It was observed that the agreement between experimental and predicted flow characteristics with zonal modelling was very good for most of the flow characteristics namely the three components of the velocity and the turbulent kinetic energy. The predictions of flow characteristics in the entire tank can be

improved further by tuning the turbulent model parameters in different zones. Therefore the k-ϵ model can successfully be used with zonal modelling for the simulation of stirred tanks. It may be interesting to note that the set of parameters chosen for pitched-blade turbine impellers holds good for other axial flow impellers such as curved pitched bladed turbine, multibladed pitched turbine, propeller and modified propeller.

List of symbols and abbreviations

C_1 empirical constant in the dissipation equation;
C_2 empirical constant in the dissipation equation;
C_D empirical constant relating eddy viscosity, k and ϵ;
CMV comparison of mean velocities;
CTP comparison of turbulent parameters;
D impeller diameter, m;
E roughness constant in wall function;
H height of liquid in the tank, m;
H_c clearance between impeller centre and vessel bottom, m;
k dimensionless turbulent kinetic energy;
$\overline{k}$ turbulent kinetic energy per unit mass, m^2/s^{-2};
P_p power calculated from power number, W;
P_e power calculated from experiment, W;
p dimensionless pressure;
R radius of the vessel, m;
r non-dimensional radial coordinate;
r_b non-dimensional distance between vessel centre and baffle edge;
r_s dimensionless radius of shaft;
S-P predicted results obtained by zonal modelling;
S_Φ source term for the generalised variable Φ;
T vessel diameter, m;
$\overline{U}$ mean velocity parallel to the wall at the near-wall node, m/s;
U_r dimensionless friction velocity;
$\overline{U}_r$ friction velocity, m/s;
U_{tip} impeller tip velocity, m/s;
u dimensionless mean radial velocity;
u' fluctuating component of the radial component of velocity, m/s;
v dimensionless mean axial velocity;
v' fluctuating component of the axial component of velocity, m/s;
w dimensionless mean tangential velocity;
w_s dimensionless tangential velocity at shaft surface;
y dimensionless local coordinate normal to the wall;
$\overline{y}$ local coordinate normal to the wall, m;
y^+ wall Reynolds number
Z-P predicted results obtained by standard set of turbulence model parameters;
z non-dimensional axial coordinate.

Greek symbols

α_e under relaxation parameter for eddy viscosity;
α_k under relaxation parameter for turbulent kinetic energy;
α_p under relaxation parameter for pressure;
α_u under relaxation parameter for velocities;
α_ϵ under relaxation parameter for turbulent energy dissipation rate;
Γ_{eff} effective viscosity for the variable Φ;
γ von Karman constant;
ϵ dimensionless turbulent energy dissipation rate;
ϵ_{av} dimensionless average dissipation rate;
θ tangential coordinate;
μ dimensionless parameter;
$\overline{\mu}$ viscosity, Pa.s;
μ_{eff} dimensionless effective viscosity, $(\mu + \mu_t)$;
μ_t non-dimensional eddy viscosity;
ρ density of water, kg/m^3;
σ_k Prandtl number for turbulent kinetic energy;
σ_ϵ Prandtl number for turbulent kinetic energy dissipation rate;
Φ generalised notation for transport variable;
$\overline{\tau_w}$ wall stress, N m^{-2};

Subscript

p denotes the values of the variables at the node point nearest to the wall.

References

Abujelala M T, Lilley D G 1984 Limitations and empirical extensions of the k-ϵ model as applied to turbulent confined swirling flows. *Chem. Eng.Commun.* 31: 223–236

Armenante P M, Chou C-C 1996 Velocity profiles in a baffled vessel with single or double pitched blade turbines. *AIChE J.* 42: 42–54

Bakker A, Van den Akker H E A 1994 Single-phase flow in stirred reactors. *Trans. Inst. Chem. Eng.* 72: 583–593

Brucato A, Ciofalo M, Grisafi F, Micale G 1994 Complete numerical solution of flow fields in baffled stirred vessels: The inner-outer approach. *Proceedings Inst. Chem. Eng. Symposium series* (136): 155–162

Desouza A, Pike R W 1972 Fluid dynamics and flow patterns in stirred tanks with a turbine impeller. *Can. J. Chem. Eng.* 50: 15–23

Drbohlav J, Fort I, Maca K, Placek J 1978 Turbulent characteristics of discharge flow from turbine impeller. *Collect. Czech. Chem. Commun.* 43: 3148–3162

Dutta S, Acharya S 1993 Heat transfer and flow past a backstep with the nonlinear k-ϵ turbulence model and the modified k-ϵ turbulence model. *Numer. Heat Transfer* 23: 281–301

Elkaim D, Reggio M, Camarero R 1993 Control volume finite element solution of a confined turbulent diffusion flame. *Numer. Heat Transfer* 23: 259–279

Ferziger J H, Kline S J, Avva R K, Bordalo S N, Tzuoo K L 1988 Zonal modelling of turbulent flows – Philosophy and accomplishments: Near-wall turbulence. *Zoran Zaric Memorial Conference* (eds) S J Kline, N H Afgan (Hemisphere) pp 801–817

Fokema M D, Kresta S M, Wood P E 1994 Importance of using the correct impeller boundary conditions for CFD simulations of stirred tanks. *Can. J. Chem. Eng.* 72: 177–183

Fort I 1967 Studies on mixing XIX – pumping capacity of propeller mixer. *Collect. Czech. Chem. Commun.* 32: 3663–3678

Fort I 1986 Flow and turbulence in vessels with axial impeller. *Mixing theory and practice* (eds), V W Uhl, J B Gray (New York: Academic Press) vol. 3

Fort I, Neugebauer R, Pastyrikova M 1971 Studies on mixing. XXIX-Spatial distribution of mechanical energy dissipated by axial impeller in a system with radial baffles. *Collect. Czech. Chem. Commun.* 36: 1769–1793

Fort I, Vonzy M, Forstova B 1991 Distribution of turbulence characteristics in agitated systems with axial high speed impeller and baffles. *7th European Conference on Mixing* 1: 33–41

Harris C K, Roekaerts D, Rosendal F J J 1996 Computational fluid dynamics for chemical reactor engineering. *Chem. Eng. Sci.* 51: 1569–1594

Harvey P S, Greaves M G 1982a Turbulent flow in an agitated vessel. Part I: a predictive model. *Trans. Inst. Chem. Eng.* 60: 195–200

Harvey P S , Greaves M G 1982b Turbulent flow in an agitated vessel. Part II: Numerical solution and model predictions. *Trans. Inst. Chem. Eng.* 60: 201–210

Hockey R M , Nouri J M 1996 Turbulent flow in a baffled vessel stirred by a 60° pitched blade impeller. *Chem. Eng. Sci.* 51: 4405–4421

Jaworski Z, Fort I 1991 Energy dissipation rate in a baffled vessel with pitched blade turbine impeller. *Collect. Czech. Chem. Commun.* 56: 1856–1867

Jaworski Z, Nienow A W, Koutsakos E, Dyster K, Bujalski W 1991 An LDA study of the turbulent flow in a baffled vessel agitated by a pitched blade turbine. *Chem. Eng. Res. Des.* 69: 313–320

Kresta S M, Wood P E 1993a The mean flow field produced by a 45 degree pitched blade turbine: Changes in the circulation pattern due to off bottom clearance. *Can. J. Chem. Eng.* 71: 42–53

Kresta S M, Wood P E 1993b The flow field produced by a pitched blade turbine : Characterization of the turbulence and estimation of the dissipation rate. *Chem. Eng. Sci.* 48: 1761–1774

Launder B E, Spalding D B 1974 The numerical computation of turbulent flows. *Comput. Methods Appl. Mech. Eng.* 3: 269–289

Obi S, Peric M 1991 Second moment calculation procedure for turbulent flows with collocated variable arrangement. *AIAAJ.* 29: 585–590

Patankar S V 1980 *Numerical heat transfer and fluid flow* (New York: Hemisphere)

Patel V C, Rodi W, Scheuerer G 1986 Turbulence models for near wall and low Reynolds number flows: A review. *AIAA J.* 23: 1308–1319

Peaceman D, Rachford H H 1955 The solution of parabolic and elliptic differential equations. *J. Soc. Ind. Appl. Math.* 3: 28–41

Peric M, Kessler R, Schellerer G 1987 Comparison of finite volume numerical methods with staggered and non-staggered grids. Report no. 163/T/87, Lehrst. für. Stromungsmechanik, Univ. Erlangen-Nbg

Pericleous K A, Patel M K 1987 The modelling of tangential and axial agitators in chemical reactors. *Phys.-Chem. Hydrodyn.* 8: 105–123

Placek J, Fort I, Strek F, Jaworski Z, Karcz Z 1978 Velocity field at the wall of fully baffled vessel with turbine impeller. *Proceedings of the 5th Congress CHISA* (Prague: Czechslovak Soc. Chem. Eng.) pp 272–285

Platzer B 1981 A contribution to the evaluation of turbulent flow in baffled tanks with radial outflow impellers. *Chem. Tech. (Liepzig)* 33: 16–19

Platzer B, Noll G 1981 An analytical solution for the flow in baffled vessel with radial outflow impellers. *Chem. Tech. (Liepzig)* 33: 648–655

Ranade V V, Dommeti S M S 1996 Computational snapshot of flow generated by axial impellers in baffled stirred vessels. *Trans. Inst. Chem. Eng.* 74: 476–484

Ranade V V, Joshi J B 1989 Flow generated by pitched blade turbines I: Measurements using laser Doppler anemometer. *Chem. Eng. Commun.* 81: 197–224

Ranade V V, Joshi J B 1990 Flow generated by a disc turbine: Part I. Experimental. *Chem. Eng. Res. Des.* 68: 19–33

Ranade V V, Joshi J B, Marathe A G 1989 Flow generated by pitched blade turbines. II: Simulation using k-ϵ model. *Chem. Eng. Commun.* 81: 225–248

Ranade V V, Bourne J R, Joshi J B 1991 Fluid mechanics and blending in agitated tanks. *Chem. Eng. Sci.* 46: 1883–1893

Ranade V V, Mishra V P, Saraph V S, Deshpande G B, Joshi J B 1992 Comparison of the axial flow impellers using laser Doppler anemometer. *Ind. Eng. Chem. Res.* 31: 2370–2379

Rodi W 1993 *Turbulence models and their application in hydraulics (Monograph)* (Rotterdam: A A Balkema)

Sahu A K, Joshi J B 1995 Simulation of flow in stirred vessels with axial flow impellers: Effects of various numerical schemes and turbulence model parameters. *Ind. Eng. Chem. Res.* 34: 626–639

Sahu A K, Kumar P, Joshi J B 1998 Simulation of flow in stirred vessel with axial flow impeller: Zonal modelling and optimization of parameters. *Ind. Eng. Chem. Res.* 37: 2116–2130

Tatterson G B, Yuan H S, Brodkey R S 1980 Stereoscopic visualisation of the flows for pitched blade turbines. *Chem. Eng. Sci.* 35: 1369–1375

Xu Y, Mcgrath G 1996 CFD predictions in stirred tank flows. *Trans. Inst. Chem. Eng.* 74: 471–475